ARTICLE

SRC and ERK cooperatively phosphorylate DLC1 and attenuate its Rho-GAP and tumor suppressor functions

Brajendra K. Tripathi[1], Meghan F. Anderman[1], Xiaolan Qian[1], Ming Zhou[2], Dunrui Wang[1], Alex G. Papageorge[1], and Douglas R. Lowy[1]

SRC and ERK kinases control many cell biological processes that promote tumorigenesis by altering the activity of oncogenic and tumor suppressor proteins. We identify here a physiological interaction between DLC1, a focal adhesion protein and tumor suppressor, with SRC and ERK. The tumor suppressor function of DLC1 is attenuated by phosphorylation of tyrosines Y451 and Y701 by SRC, which down-regulates DLC1's tensin-binding and Rho-GAP activities. ERK1/2 phosphorylate DLC1 on serine S129, which increases both the binding of SRC to DLC1 and SRC-dependent phosphorylation of DLC1. SRC inhibitors exhibit potent antitumor activity in a DLC1-positive transgenic cancer model and a DLC1-positive tumor xenograft model, due to reactivation of the tumor suppressor activities of DLC1. Combined treatment of DLC1-positive tumors with SRC plus AKT inhibitors has even greater antitumor activity. Together, these findings indicate cooperation between the SRC, ERK1/2, and AKT kinases to reduce DLC1 Rho-GAP and tumor suppressor activities in cancer cells, which can be reactivated by the kinase inhibitors.

Introduction

The *SRC* gene is the prototypic member of the *SRC* family kinases (SFKs), whose nine members encode nonreceptor tyrosine-protein kinases that share a similar structure and have key roles in normal physiology and cancer (Sen and Johnson, 2011). Three of the SFKs—*SRC*, *FYN*, and *YES*—are widely expressed. Despite their partial genetic redundancy, inactivation of any two of these genes results in severe developmental defects (Lowell and Soriano, 1996). In neoplasia, where the demands of abnormal growth may be greater than during normal development, the requirement for endogenous WT SRC alone for full oncogenicity can be readily demonstrated (Guy et al., 1994). The SRC protein is implicated in several tumorigenic processes, including key roles in regulating integrin signaling, cytoskeletal organization, and adhesion dynamics, and increased SRC activity is associated with integrin activation, disruption of actin stress fibers, and disassembly of focal adhesions (Fincham et al., 1999; Klinghoffer et al., 1999; Frame et al., 2002; Webb et al., 2004). SRC also positively regulates the RhoA GTPase, which is frequently activated in advanced cancer (Ellenbroek and Collard, 2007). Many of the previously identified SRC and SFK substrates are pro-oncogenic proteins, such as FAK, p130Cas, Cortactin, and c-RAF, whose phosphorylation by SRC increases their activity, or substrates whose consequences for tumorigenesis have not been clearly established (Reynolds et al., 2014; Sulzmaier et al.,

2014; Takahashi et al., 2017). In addition, SRC phosphorylation of other targets, such as PP2A and caveolin-1, can attenuate their tumor suppressor activities.

The serine/threonine kinases ERK1 and ERK2, which are key components of the RAS-RAF-MEK-ERK pathway, phosphorylate several substrates with diverse cellular functions (Yoon and Seger, 2006; Buscà et al., 2016). For example, ERK phosphorylation of some proteins, such as FOS and JUN, helps orchestrate the cell transcription program. In other proteins, such as SOS1, B-RAF, and MEK, the phosphorylation attenuates upstream activators of ERK1/2. In still others, such as BAD and caspase-9, it can reduce their pro-apoptotic activity.

DLC1 is a tumor suppressor gene that is required for embryonic development (Durkin et al., 2007) and is down-regulated in a variety of malignancies through genetic and epigenetic modifications (Durkin et al., 2007; Lukasik et al., 2011; Barras and Widmann, 2014; Ko and Ping Yam, 2014; Wang et al., 2016). The DLC1 protein possesses a Rho-GAP (GTPase-activating protein) activity, which negatively regulates Rho GTPases by catalyzing the hydrolysis of their active GTP-bound form to their inactive GDP-bound form (Wong et al., 2005). DLC1 localizes to focal adhesions, whose turnover is RhoA dependent. RhoA, which is required for embryonic development (Zhou and Zheng, 2013) and regulates cell proliferation, cytoskeletal dynamics, cell

[1]Laboratory of Cellular Oncology, National Cancer Institute, National Institutes of Health, Bethesda, MD;   [2]Laboratory of Proteomics and Analytical Technologies, Frederick National Laboratory for Cancer Research, Frederick, MD.

Correspondence to Douglas R. Lowy: lowyd@mail.nih.gov;   Brajendra K. Tripathi: tripathib@mail.nih.gov;   M. Zhou's present address is Inova Schar Cancer Institute, Falls Church, VA.

migration, and cytokinesis, is frequently activated in advanced cancer, where it contributes to maintenance of the oncogenic phenotype (Wong et al., 2005; Wang et al., 2016). In addition to its Rho-GAP activity, the DLC1 protein has scaffold functions, including the binding of tensins, talin, FAK, and caveolin-1. Both the catalytic and scaffold activities contribute to the tumor suppressor functions of DLC1.

There is no previously known relationship between DLC1 and SRC/SFKs or ERK, but we report here that DLC1 is a critical physiological substrate for SRC/SFKs and ERK, which directly phosphorylate DLC1 and attenuate its Rho-GAP and tumor suppressor activities. Our observations are noteworthy because the regulation of DLC1 by SRC/SFKs makes an important contribution to the physiology of SRC/SFKs and to the growth control of DLC1-expressing tumors, and may have translational implications.

Results

SRC kinase increases RhoA-GTP in a DLC1-dependent manner

In a survey of nontransformed and cancer-derived cell lines, we unexpectedly found an excellent correlation between levels of RhoA-GTP, total SRC protein, and SRC activity (as monitored by SRC-Y416 phosphorylation), an inverse correlation with DLC1 protein levels, and no correlation with p190–Rho-GAP (Fig. 1, A and B; and Fig. S1, A and B, for quantitation of DLC1 and SRC protein levels). To explore a possible mechanistic relationship between SRC, RhoA-GTP, and DLC1, we treated two DLC1-positive (H1703 and H157) and two DLC1-negative (H358 and A549) non–small cell lung cancer (NSCLC) lines with the SRC inhibitor saracatinib, which reduced RhoA-GTP in both DLC1-positive lines, but not in the DLC1-negative lines (Fig. 1, C–F). Similarly, treatment of the two DLC1-positive lines with the tyrosine kinase inhibitor bosutinib (Fig. S1, C and D) or SRC siRNAs (Fig. S1, E and F) led to decreased RhoA-GTP. Transfection of H1703 with WT SRC increased RhoA-GTP, while transfection with kinase-dead SRC decreased RhoA-GTP, presumably because of its dominant-negative activity (Fig. S1, G and H; Destaing et al., 2008). Taken together, these results indicate SRC kinase can increase RhoA-GTP in DLC1-positive, but not in DLC1-negative, lines.

To directly establish the role of DLC1, we tested the effect of DLC1 depletion by siRNAs on the ability of saracatinib to affect the RhoA-GTP level in two DLC1-positive lines, H1703 and H157. This reduction in DLC1, which increased RhoA-GTP as expected, abolished the ability of saracatinib to down-regulate RhoA-GTP in both lines (Fig. 1 G and Fig. S1 I). Conversely, the forced expression of DLC1 in a DLC1-negative line, H358, which reduced RhoA-GTP as expected, enabled saracatinib to further decrease RhoA-GTP (Fig. 1 H). Thus, SRC regulation of RhoA-GTP under these conditions depends upon DLC1. Although SRC can phosphorylate p190–Rho-GAP (Moran et al., 1991), this gene was not involved in the SRC-dependent regulation of RhoA-GTP identified here, as p190–Rho-GAP depletion by siRNAs did not affect the ability of saracatinib to reduce RhoA-GTP in a DLC1-positive line, H1703 (Fig. S1 J).

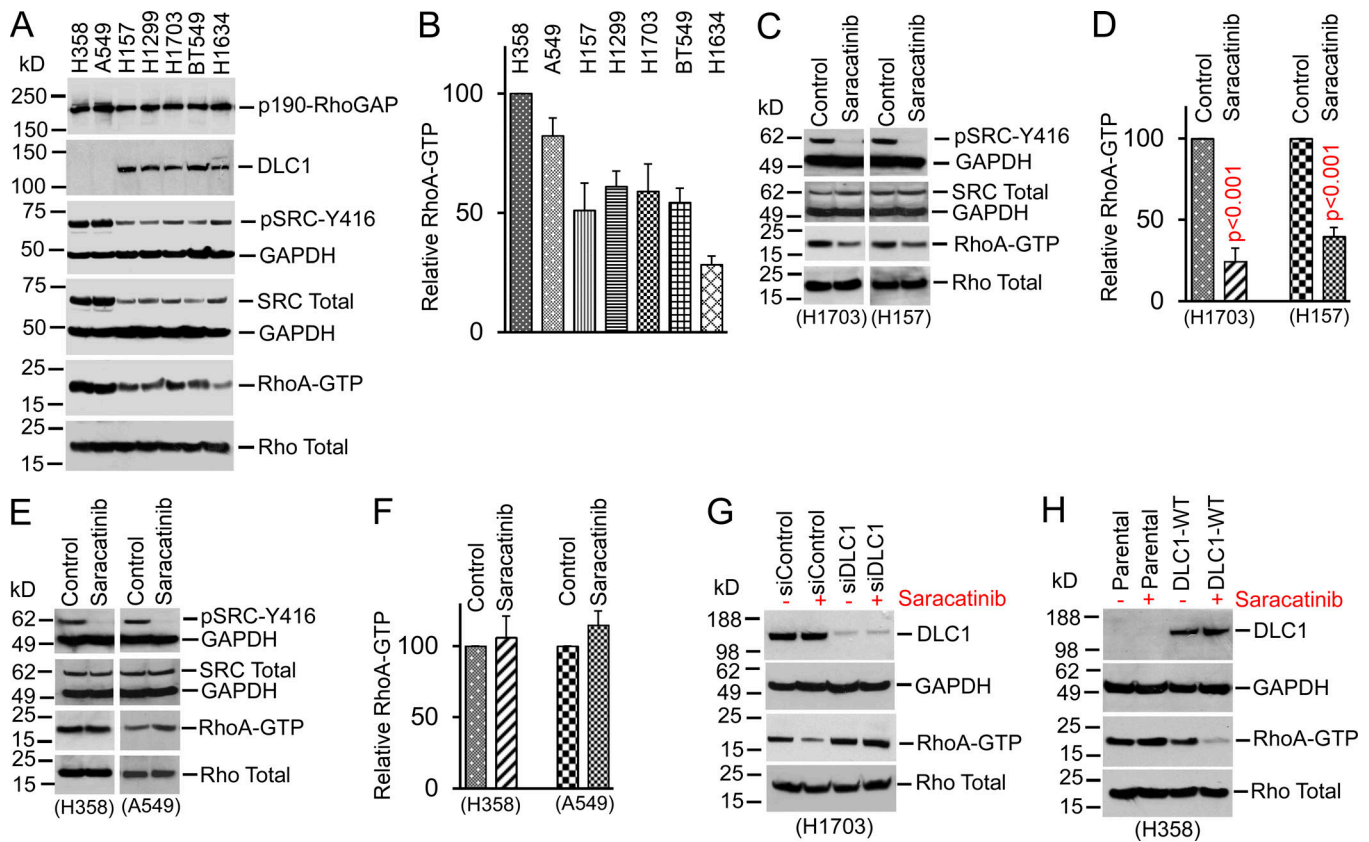### Kinase-active SRC forms an endogenous complex with DLC1

To determine if SRC and DLC1 form an endogenous protein complex, we performed coimmunoprecipitation (coIP) experiments in two NSCLC lines, H157 and H1703. SRC and DLC1 formed a protein complex in both lines, whether cell lysates were immunoprecipitated (IP) first with a DLC1 antibody and then immunoblotted (IB) for SRC (Fig. 2 A) or by the reciprocal coIP (Fig. 2 B). A majority of the SRC protein associated with DLC1 was enzymatically active, as saracatinib reduced most of the coIP total SRC (Fig. 2 C) and kinase-active SRC (Fig. 2 D). Complex formation between SRC and DLC1 was also observed in the nontransformed H2071 and human bronchial epithelial cell (HBEC) lines (Fig. 2 E), which implies the interaction is physiologically relevant.

Colocalization of SRC and DLC1 was confirmed by confocal microscopy in H1703 and H157 cells, with colocalization coefficients of 0.66 and 0.62, respectively (Fig. 2 F and Fig. S2 A), and with positive proximity ligation assays (PLAs; Fig. 2 G and Fig. S2 B). Colocalization of kinase-active SRC at focal adhesions, as monitored with vinculin, was confirmed in H1703 and H157 cells, with colocalization coefficients of 0.72 and 0.66, respectively (Fig. 2 H and Fig. S2 C), and with positive PLA (Fig. 2 I and Fig. S2 D). Consistent with this finding, SRC and vinculin were not colocalized in a DLC1-negative line (H358; data not shown). Thus, colocalization of SRC at focal adhesions depends on the presence of DLC1.

Increased RhoA-GTP by fibronectin-induced SRC activity is mediated by DLC1

The above results, conducted under steady-state growth conditions, led us to explore whether a physiological, inducible situation that can stimulate SRC activity and increase RhoA-GTP might also depend on DLC1. To test this possibility, we placed six different cell lines on culture dishes that had been coated with the integrin ligand fibronectin, which can activate SRC (Harburger and Calderwood, 2009) and increase RhoA-GTP (Ren et al., 1999). To determine if the response would be relevant to nontransformed cells and cancer cells, two of the DLC1-positive lines, H1634 and H2071, were nontransformed and expressed DLC1, while the other four were NSCLC lines, the two DLC1-positive and two DLC1-negative ones studied above. Plating the cells on fibronectin led to SRC activation in all six lines as expected, but the increase in RhoA-GTP was limited to the four DLC1-positive lines (Fig. 3, A–F). The inability of SRC to increase RhoA-GTP in the two DLC1-negative lines was not attributable to their RhoA-GTP levels being maximal, as lysophosphatidic acid (LPA), which increases RhoA-GTP through activation of large G protein–coupled receptors (Xiang et al., 2013), increased RhoA-GTP in both lines when plated on fibronectin, as well as in the DLC1-positive H1634 line (Fig. S2, E and F).

The increased RhoA-GTP depended on the SRC activation by fibronectin, as saracatinib prevented SRC activation and increased RhoA-GTP (Fig. 3 G). Plating cells on fibronectin can also increase FAK activity (Meng et al., 2009), but treatment with a FAK kinase inhibitor, FAK-14, did not interfere with either fibronectin-induced SRC activation or increased RhoA-GTP, although it did inhibit FAK activity, as monitored by reduced

Tripathi et al.
SRC inhibitors reactivate the tumor suppressor DLC1

Journal of Cell Biology
https://doi.org/10.1083/jcb.201810098

3061

Figure 1. SRC activity increases RhoA-GTP through DLC1. (A) Relative protein expression of p190–Rho-GAP, DLC1, kinase-active SRC (pSRC-Y416), total SRC, RhoA-GTP, and total Rho in the indicated lines. The quantification for DLC1 and SRC is shown in Fig. S1, A and B. GAPDH was used a loading control. DLC1-positive lines show lower RhoA-GTP than DLC1-negative lines. **(B)** Graph shows relative RhoA-GTP ± SD from three experiments. **(C–F)** Saracatinib decreases RhoA-GTP in DLC1-positive lines (H1703 and H157), but not in DLC1-negative lines (H358 and A549). Each graph shows relative RhoA-GTP ± SD from three experiments. **(G)** DLC1 knockdown by siRNAs abrogates the ability of saracatinib to suppress RhoA-GTP in H1703 cells. **(H)** Saracatinib does not affect RhoA-GTP in parental DLC1-negative H358 cells, but stable transfection of DLC1 decreases basal RhoA-GTP and enables saracatinib to further reduce RhoA-GTP.

FAK-Y397 phosphorylation (Fig. 3 G). The increased RhoA-GTP required DLC1 protein, as siRNAs depletion of DLC1 abrogated the ability of fibronectin to increase RhoA-GTP (Fig. 3 H). SRC activation by fibronectin treatment led to increased tyrosine phosphorylation of DLC1, which was markedly reduced by sar-acatinib treatment, but not by FAK-14 treatment (Fig. S2, G–J). Fibronectin and saracatinib treatment did not alter SRC protein level, and fibronectin treatment did not alter the FAK activity. Thus, the fibronectin-induced increase in RhoA-GTP requires SRC activation and the presence of DLC1, and is associated with the phosphorylation of one or more tyrosines in DLC1.

Kinetic analysis of the fibronectin-induced activities indicated that SRC-Y416 phosphorylation began within 15 min of plating, while the increased RhoA-GTP and tyrosine phosphorylation of DLC1 began at ~30 min (Fig. 3, I and J). The latter two increases were correlated with increased SRC/DLC1 complex formation between 15 and 30 min (Fig. S2 K).

SRC interacts with two regions of DLC1 and directly phosphorylates DLC1 tyrosines 451 and 701
DLC1 has four recognized regions: an N-terminal SAM domain, a linker region, a Rho-GAP domain, and a C-terminal START domain (Fig. 4 A). To identify the regions of DLC1 required for SRC

binding, lysates from human embryonic kidney (HEK) 293T cells expressing various GFP-tagged DLC1 fragments (Fig. 4 A) were IP with SRC antibody followed by IB with GFP antibody. Inter-estingly, SRC bound two nonoverlapping DLC1 fragments, one spanning amino acids 1–492 and the other 500–1,091, implying that SRC interacts with more than one DLC1 region (Fig. 4 B). The N-terminal binding region of DLC1 was mapped more pre-cisely to DLC1 amino acids 80–200 (Fig. 4 C). DLC1 amino acids 800–850, in the Rho-GAP domain, were required for SRC binding the C-terminal region, as both DLC1(800–900) and DLC1(609–850) were positive, while DLC1(850–1,091) was neg-ative (Fig. 4, D and E).

As had been true following the plating of cells on fibronectin, tyrosine in DLC1 was phosphorylated in a SRC-dependent manner under steady-state growth conditions, as saracatinib reduced DLC1 tyrosine phosphorylation in H1703 and H157 lines (Fig. 4 F). To map the phosphorylated DLC1 tyrosine residues, liquid chromatography–mass spectrometry (LCMS) was per-formed with partially purified DLC1 protein from HEK 293T cells transfected with DLC1 alone or cotransfected with constitutive kinase-active or kinase-dead SRC (Fig. 4 G and Fig. S3 A). The LCMS results support the conclusion that DLC1-Y451 and -Y701 are phosphorylated in a SRC-dependent manner, as LCMS
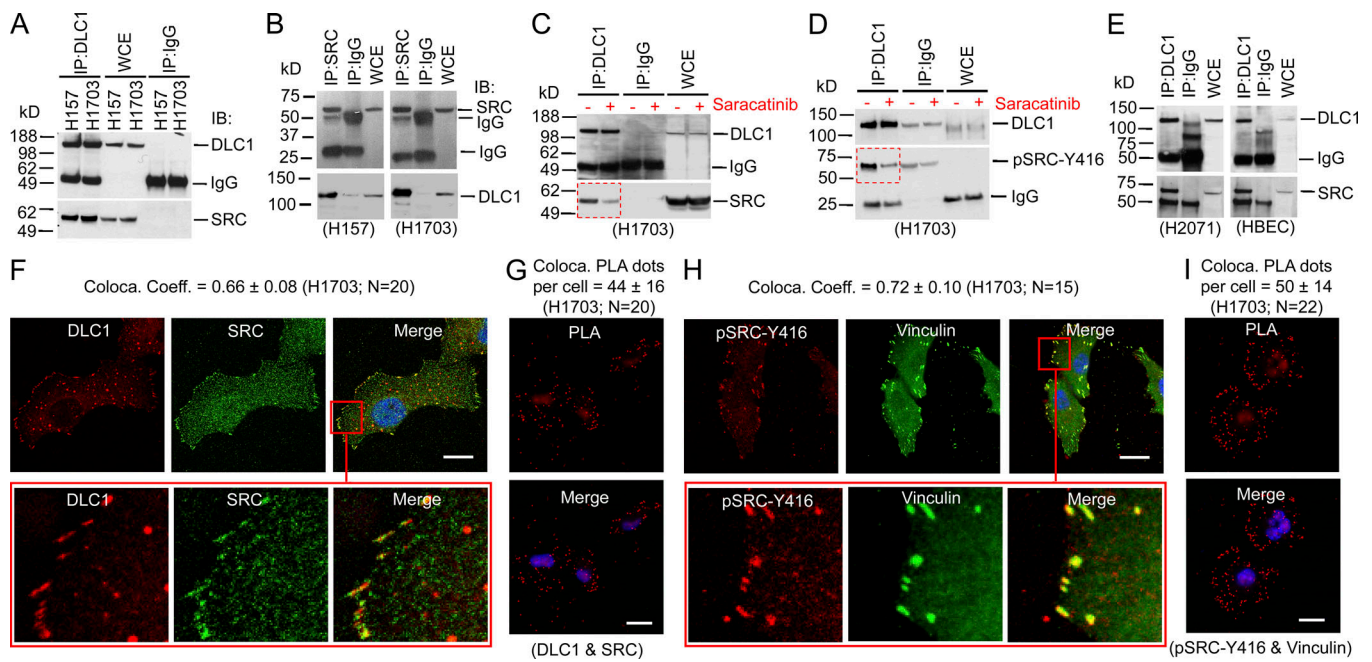
Figure 2. **Kinase active SRC binds to DLC1. (A)** Stable protein complex between DLC1 and SRC. Lysates from H157 and H1703 cells were IP with DLC1 or mock IgG antibodies followed by IB with DLC1 (top) or SRC (bottom) antibodies. WCE, whole cell extract. **(B)** Complex between DLC1 and SRC is confirmed by reciprocal coIP. Lysates from H157 and H1703 cells were IP with SRC or mock IgG antibodies followed by IB with SRC (top) or DLC1 (bottom) antibodies. **(C)** Saracatinib treatment reduced the total amount of SRC protein in complex with DLC1 (highlighted in red-dotted rectangle). **(D)** Protein complex between DLC1 and kinase-active SRC (pSRC-Y416) is reduced (highlighted in red-dotted rectangle) by saracatinib. **(E)** Complex between DLC1 and SRC in nontransformed H2071 and HBEC cell lines. **(F)** Colocalization of SRC with DLC1. H1703 cells were stained with DLC1 (red) and SRC (green) antibodies. Colocalization of DLC1 and SRC is highlighted in red box. Red box in the merge image is a zoomed-in view of the selected area that highlights the colocalization between DLC1 (red) and SRC (green). Averaged overlapping colocalization coefficient ± SD was calculated from 20 cells randomly selected from several fields. Scale bar, 20 µm. **(G)** Colocalization of DLC1 and SRC was confirmed by PLA. Scale bar, 20 µm. **(H)** Colocalization of kinase active SRC with vinculin. H1703 cells were stained with kinase active SRC (pSRC-Y416) (red) and vinculin (green) antibodies. Colocalization of pSRC-Y416 and vinculin is highlighted in red box. Red box in the merge image is a zoomed-in view of the selected area that highlights the colocalization between pSRC-Y416 (red) and vinculin (green). Averaged overlapping co-localization coefficient ± SD was calculated from 15 cells randomly selected from several fields. Scale bar, 20 µm. **(I)** Colocalization of kinase-active SRC (pSRC-Y416) and vinculin was confirmed by PLA. Scale bar, 20 µm.

detected strong phosphorylation that was fully localized on Y451 and Y701 in the relevant DLC1-WT peptides in the samples from cells expressing constitutively kinase-active SRC, but not from cells expressing kinase-dead SRC.

To establish that SRC directly phosphorylates DLC1, we performed an in vitro kinase assay using ^{32}P labeling. Partially purified GFP-DLC1-WT was strongly phosphorylated by recombinant SRC in vitro, unlike the GFP control (Fig. 4 H, lanes 2 and 3), and saracatinib treatment abolished the phospho-signal in GFP-DLC1-WT (Fig. S3 B). Thus, DLC1 is a direct SRC substrate. Furthermore, DLC1 fragments spanning amino acids 1–492 and 500–1091, which contain Y451 and Y701, respectively, were strongly phosphorylated (Fig. S3 C). Recombinant SRC also phosphorylated the other two members of DLC family, DLC2 and DLC3, but less strongly than DLC1 (Fig. S3 D).

To confirm that Y451 and Y701 are the major SRC phosphorylation sites in DLC1, both tyrosines were mutated to the phospho-deficient phenylalanine (DLC1-2F), which drastically reduced, but did not abolish, the phospho-signal (Fig. 4 H, lane 6). When tyrosine-to-phenylalanine single mutants were analyzed, the phospho-signal was reduced, but was greater than the DLC1-2F mutant (Fig. 4 H, lanes 4 and 5). The two other widely expressed SFKs, FYN and YES, also directly phosphorylate DLC1

(Fig. 4 I). As with SRC, the phospho-signal by FYN kinase was much lower when the DLC1-2F mutant was tested in an analogous in vitro kinase assay (Fig. S3 E).

ERK phosphorylation of DLC1-S129 increases SRC SH3 binding to DLC1 and phosphorylation of Y451 and Y701

The LCMS analysis of DLC1 phosphorylations indicated that S129 was phosphorylated (Fig. 4 G). Inspection of the sequences surrounding S129 indicated this serine might be part of overlapping consensus motifs for ERK1/2 phosphorylation (127-PXSP-130) and SH3 domain binding (127-PXXP-130). As SRC binding had been mapped to DLC1 amino acids 80–200 (Fig. 4 C), we investigated the possibility that the SRC SH3 domain might bind to this fragment, that S129 might be phosphorylated by ERK, and that this phosphorylation might affect the putative SH3 binding. CoIP of extracts from the H157 and H1703 lines determined that ERK and DLC1 formed an endogenous protein complex (Fig. 5, A and B). Furthermore, the SRC SH3 domain did bind DLC1 amino acids 80–200 in vivo, and it bound the full-length DLC1-WT more strongly than it bound the full-length DLC1-S129A mutant (Fig. 5, C and D). Similarly, an in vitro ERK kinase assay gave a strong phospho-signal with full-length DLC1-WT or DLC1 amino acids 80–200, but a greatly attenuated
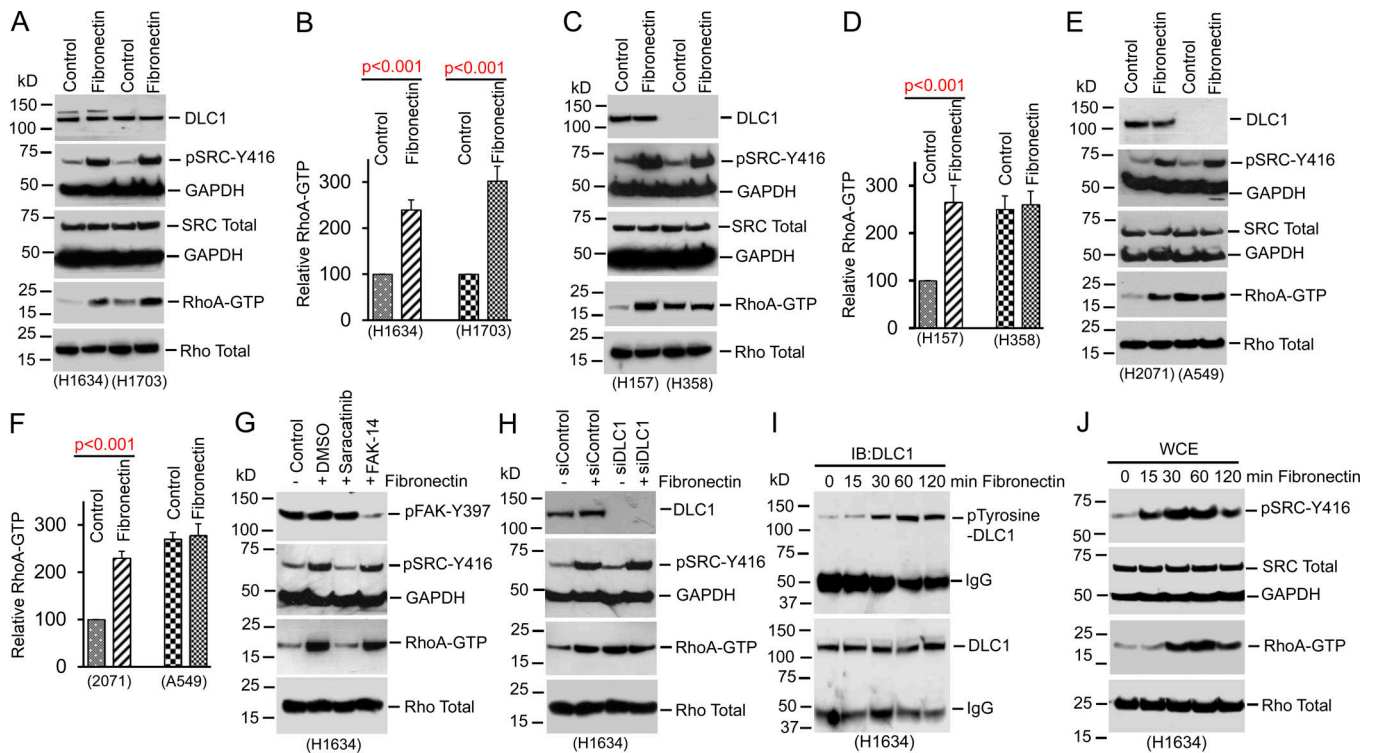
Figure 3. **Fibronectin-induced SRC activity increases RhoA-GTP through DLC1. (A–F)** Fibronectin increases SRC activity and RhoA-GTP, but not total SRC and total Rho, in DLC1-positive nontransformed (H1634 and H2071) and in cancer (H1703 and H157) lines. Fibronectin increases SRC activity in DLC1-negative (H358 and A549) lines, but does not alter RhoA-GTP in the lines. Graphs in panels B, D, and F show relative RhoA-GTP ± SD from three experiments, as shown in A, C, and E, respectively. Parametric two-tailed *t* tests were performed for statistical analysis. **(G)** SRC inhibitor saracatinib, but not FAK inhibitor FAK-14, decreases RhoA-GTP induced by fibronectin. **(H)** DLC1 knockdown abrogates the ability of fibronectin to increase RhoA-GTP. Fibronectin increases RhoA-GTP in DLC1-positive cells, but not in DLC1-knockdown cells, although fibronectin increases SRC activity in both conditions. **(I)** Fibronectin increases tyrosine phosphorylation of DLC1 (pTyrosine) over time without changing total DLC1. Lysates from fibronectin-treated H1703 cells at the indicated time points were IP with DLC1 antibodies followed by IB with pTyrosine (top) or DLC1 (bottom) antibodies. **(J)** Fibronectin induces SRC activity after 15 min and increased RhoA-GTP after 30 min, which correlates with increased tyrosine phosphorylation of DLC1 at 30 min (I).

phospho-signal for the S129A mutant in both the full-length and 80–200 DLC1 fragment (Fig. 5, E and F). Importantly, the in vitro SRC kinase reaction gave a stronger DLC1 tyrosine phosphorylation signal with DLC1-WT than with the DLC1-S129A mutant, indicating the ERK-dependent phosphorylation of S129 increases the efficiency of SRC-dependent phosphorylation of Y451 and Y701 (Fig. 5 G). Thus, ERK-dependent phosphorylation of S129 increases the efficiency of SRC binding via its SH3 domain, which in turn increases phosphorylation of Y451 and Y701.

SRC phosphorylation of DLC1-Y451 decreases tensin binding to DLC1

The DLC1 scaffold functions include its binding of talin, FAK, and tensin near residue Y451. Tensin binding requires a DLC1 segment that includes residues 440–445 (Liao et al., 2007; Qian et al., 2007), while both FAK and talin bind DLC1 residues 467–489 (Li et al., 2011; Zacharchenko et al., 2016). To determine if phosphorylation of Y451 affects tensin binding, GST-tagged full-length tensin was cotransfected with a DLC1 fragment encoding WT amino acids 80–550, with the same fragment encoding Y451F phospho-deficient mutant, or with the phosphomimetic Y451D mutant, and GST pull-downs were analyzed for binding the expressed DLC1 segment. Compared with tensin

binding to DLC1-WT, the DLC1-Y451F mutant bound tensin more efficiently, while the DLC1-Y451D mutant bound it less efficiently (Fig. 5 H). Analogous results were seen when the tensin fragment (amino acids 1508–1786) shown previously to bind DLC1 was transfected with DLC1 WT or the Y451 mutants (Fig. 5 I). These observations strongly suggest that phosphorylation of Y451 decreases tensin binding. By contrast, an analogous evaluation of talin protein indicated that its binding to DLC1 was not affected by the Y451F or the Y451D mutation (Fig. 5, J and K).

SRC phosphorylation of DLC1 attenuates the Rho-GAP activity of DLC1

Our finding that SRC could increase RhoA-GTP in a DLC1-dependent manner suggested that SRC-dependent phosphorylation of DLC1 would attenuate its Rho-GAP function. Therefore, we compared the Rho-GAP activity for DLC1-WT, for the tyrosine to phenylalanine single mutants (DLC1-Y451F and DLC1-Y701F), the combined tyrosine to phenylalanine double mutant (DLC1-2F), the phosphomimetic tyrosine to aspartate single mutants (DLC1-Y451D and DLC1-Y701D), and the combined tyrosine to aspartate double mutant (DLC1-2D), and included a "Rho-GAP–dead" mutant (DLC1-R718A) as a control.
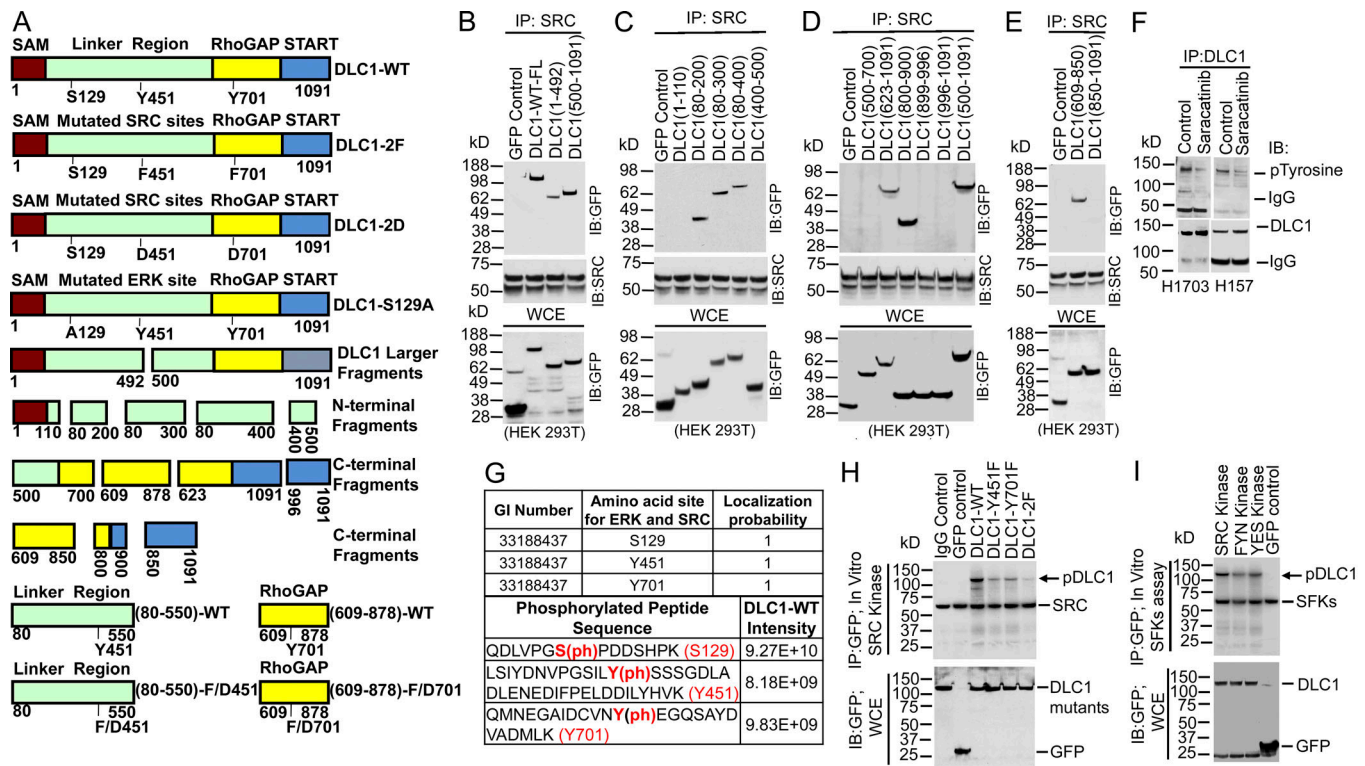
Figure 4. **SRC binds two nonoverlapping regions of DLC1 and phosphorylates two tyrosines in DLC1. (A)** Schematic representation of DLC1 domains, DLC1 mutants, and DLC1 fragments used in this study. All constructs were GFP-tagged. **(B)** SRC binds to DLC1. N-terminal and C-terminal fragments. Lysates from HEK 293T cells transfected with indicated DLC1 constructs were IP with SRC antibody followed by IB with GFP (top) and SRC (middle) antibodies. Expression of DLC1 constructs (bottom). **(C–E)** Experimental conditions were similar to B. **(C)** SRC binds to DLC1 amino acids 80–200, but not 1–110 and 400–500 N-terminal DLC1 fragments. **(D and E)** SRC binds to the Rho-GAP domain (amino acids 800–900) of DLC1, but not the C-terminal fragment (amino acids 850–1091). **(F)** Saracatinib reduces tyrosine phosphorylation of DLC1 (pTyrosine) without reducing total DLC1. Lysates from H1703 and H157 lines treated without or with saracatinib were IP with DLC1 antibodies followed by IB with pTyrosine (top) or DLC1 (bottom) antibodies. Whole cell extract (WCE) input is the same, and it is shown in Fig. 1. **(G)** Phosphorylation of DLC1 S129, Y451, and Y701 in cells. DLC1 phosphopeptides from extracts of HEK 293T cells transfected with SRC were detected by mass spectrometry. The phosphorylation signals were fully localized to the indicated serine and tyrosines in phosphopeptides. GI, GenInfo identifier number. **(H)** Recombinant SRC strongly phosphorylates DLC1-WT, from transfected HEK 293T cells, in vitro, while single mutants (DLC1-Y451F or DLC1-Y701F) were weakly phosphorylated, and phosphorylation of the combined DLC1-2F mutant (DLC1-Y451F,Y701F) was barely detectable. **(I)** Top: Two other SFKs, FYN and YES, phosphorylate DLC1, but less efficiently than SRC. Bottom: Expression of DLC1 constructs.

In A549 cells that expressed similar levels of the DLC1 mutants, RhoA-GTP levels in the DLC1-Y701D and DLC1-2D transfectants were similar to DLC1-R718A, while RhoA-GTP in the DLC1-2F mutant was even lower than that induced by DLC1-WT (Fig. 6 A). The RhoA-GTP phenotypes mapped to Y701 phosphorylation, as RhoA-GTP was high and low, respectively, for the DLC1-Y701D and DLC1-Y701F single mutants, while there was little difference in RhoA-GTP between the DLC1-Y451D and DLC1-Y451F single mutants and the DLC1-WT. Analogous results were seen when the DLC1 mutants were analyzed for two RhoA-GTP downstream effectors, Rho kinase (ROCK) activity (Fig. 6 B) and phosphorylation of myosin regulatory light chain (pMRLC), as analyzed by IB (Fig. 6 C) and immunofluorescence (Fig. S4, A and B). Consistent with these results, cells transfected with GFP, DLC1-Y701D, DLC1-2D, or DLC1-R718A had well-formed stress fibers, unlike cells transfected with DLC1-WT, DLC1-Y701F, or DLC1-2F (Fig. S4 C).

As Y701 is located in the Rho-GAP domain, we asked whether the Rho-GAP activities that were mainly attributable to amino acid encoded at residue 701 would map to the Rho-GAP domain,

which has previously been genetically mapped to DLC1(609–878; Kim et al., 2008). Consistent with this possibility, the in vivo RhoA-GTP phenotypes for the Y701 mutants of the isolated DLC1 Rho-GAP domain were similar to those with the same Y701 mutation in full-length DLC1 (Fig. 6 D). Analogous results were observed when the DLC1 full-length or isolated Rho-GAP domain mutants were analyzed for their in vitro Rho-GAP activity (GTP hydrolysis), with Y701F being most active and Y701D least active (Fig. 6, E and F). Compared with DLC1-WT, the in vitro RhoA-GTP binding to the full-length DLC1-2D mutant was as low as that of the Rho-GAP–dead DLC1-R677A mutant, whose RhoA-GTP binding is known to be reduced (Fig. 6 G; Jaiswal et al., 2014). Thus, the mutant analysis indicates that SRC phosphorylation of DLC1 attenuates its Rho-GAP activity, and this phenotype maps to Y701 and the Rho-GAP domain.

SRC phosphorylation of DLC1 attenuates its tumor suppressor functions
To examine the biological significance of DLC1 phosphorylation by SRC, we evaluated the phosphodeficient and phosphomimetic
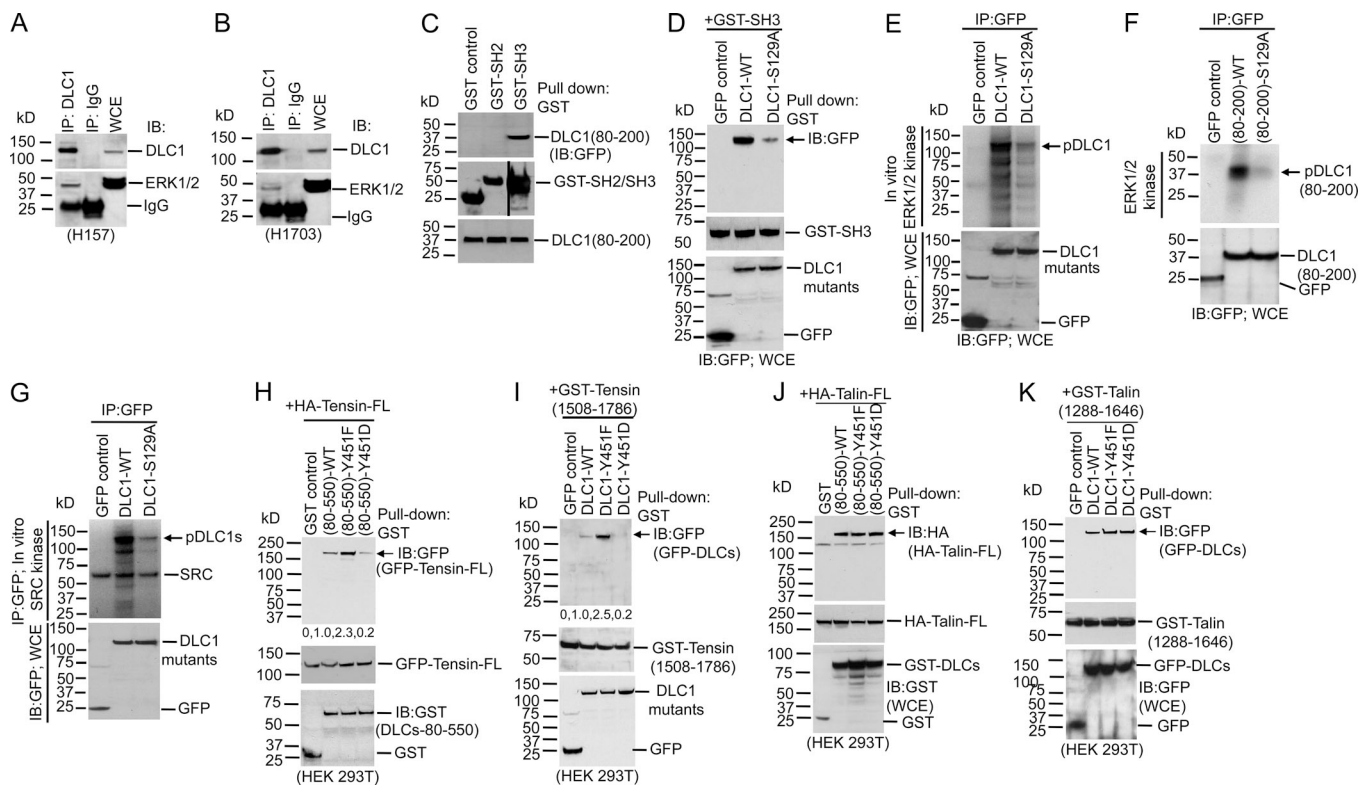
Figure 5. ERK phosphorylation of DLC1-S129 increases SRC binding; SRC phosphorylation of DLC1-Y451 decreases tensin binding to DLC1. (A and B) Protein complex between DLC1 and ERK1/2. Lysates from H157 and H1703 cells were IP with DLC1 or mock IgG antibodies followed by IB with DLC1 (top) or ERK1/2 (bottom) antibodies. **(C)** SRC SH3 binds to the 80–200 region of DLC1. **(D)** SRC SH3 binds more efficiently to DLC1-WT than to DLC1-S129A mutant. Bottom panels for D and E are the same blot for whole cell extract (WCE) input. **(E and F)** IP DLC1-WT (E) and DLC1(80–200; F) were strongly phosphorylated in vitro by recombinant ERK1/2 kinase, while DLC1-S129A (E) or DLC1(80–220)-S129A (F) were weakly phosphorylated. **(G)** IP DLC1-WT was strongly phosphorylated in vitro by recombinant SRC kinase, while DLC1-S129A was weakly phosphorylated. **(H and I)** SRC phosphorylation of DLC1-Y451 decreases the binding of tensin protein to DLC1. In HEK 293T cells, GFP-tensin-FL (H) and GST-tensin (1,508–1,786; I) bind more efficiently to DLC1-WT or DLC1-Y451F than to DLC1-Y451D mutant (top). IB with GFP (middle) or GST (bottom) antibodies shows expression of GFP-tensin or GST-tagged DLC construct. **(J and K)** The binding of talin protein to DLC1 was not affected by mutation of DLC1-Y451. **(J)** IIBs from HEK 293T cells cotransfected with HA-tagged full-length talin and GST, GST-DLC1(80–550)-WT, GST-DLC1(80–550)-Y451F, or GST-DLC1(80–550)-Y451D fragment were pulled down with GST antibody and IB with HA antibody (top). IB with HA (middle) or GST (bottom) antibodies shows expression of HA-talin or GST-tagged DLC construct. **(K)** IBs from HEK 293T cells cotransfected with GST-tagged talin (1,288–1,646) and GFP, GFP-tagged DLC1-WT, DLC1-Y451F, or DLC1-Y701D were pulled down with GST antibody and IB with GFP antibody (top). The GFP-DLC1-Y451D bound talin (1,288–1,646) fragment as efficiently as GFP-DLC1-WT or GFP-DLC1-Y451F mutant. IB with GST (middle) and GFP (bottom) antibodies shows expression of GST-tagged talin fragment and GFP-tagged DLC1 mutants.

DLC1 single and double mutants in several cancer-related bioassays. Stable DLC1-WT transfectants in the H358 line reduced the following functions: anchorage-independent cell growth (Fig. 7, A and B), transwell cell migration (Fig. 7, C and D), and xenograft tumors in immunodeficient mice (Figs. 7, E–G; and Fig. S4, D and E). In these bioassays, the DLC1-2D mutant was as deficient as the Rho-GAP–dead DLC1-R718A, while the DLC1-2F mutant was even more active than DLC1-WT.

SRC inhibitors have antitumor activity in DLC1-WT xenografts, but not in isogenic DLC1 mutant xenografts

Given the reversibility of the SRC-dependent DLC1 phosphorylation, we evaluated whether SRC inhibitors might have therapeutic efficacy in a DLC1-positive tumor that had high SRC activity. First, we used the MMTV-PyMT breast cancer model, where the MMTV promoter drives the polyomavirus middle T antigen, which stimulates SRC activity (Guy et al., 1994). 5 d of oral treatment with saracatinib reduced breast tumor weight by

>50% (Fig. 8 A), which was correlated with decreased SRC activity and RhoA-GTP levels (Fig. 8, B and C).

To determine mechanistically if DLC1 reactivation contributes to the antitumor activity from SRC kinase inhibition, we examined the response of saracatinib treatment to tumor xenografts derived from the H358 NSCLC line in immunodeficient NOD-SCID mice by comparing four isogenic H358 cell lines that differed in the DLC1 allele they expressed: DLC1-WT, DLC1-2F, DLC1-2D, or DLC1-negative (GFP control). Saracatinib treatment for 5 d reduced tumor weight of the DLC1-WT line by 75%, in contrast to a 20% reduction for the DLC1-negative control line (Fig. 8, D and E). Similar to the DLC1-negative control, saracatinib treatment of the DLC1-2F and DLC1-2D tumors, whose DLC1 activity would be predicted to not be altered by a SRC inhibitor, reduced tumor weight by 18% and 21%, respectively. The results with the DLC1-2F and DLC1-2D mutants, which should not be reactivatable by the SRC inhibitor because their tyrosine residues have been mutated, strongly imply that the
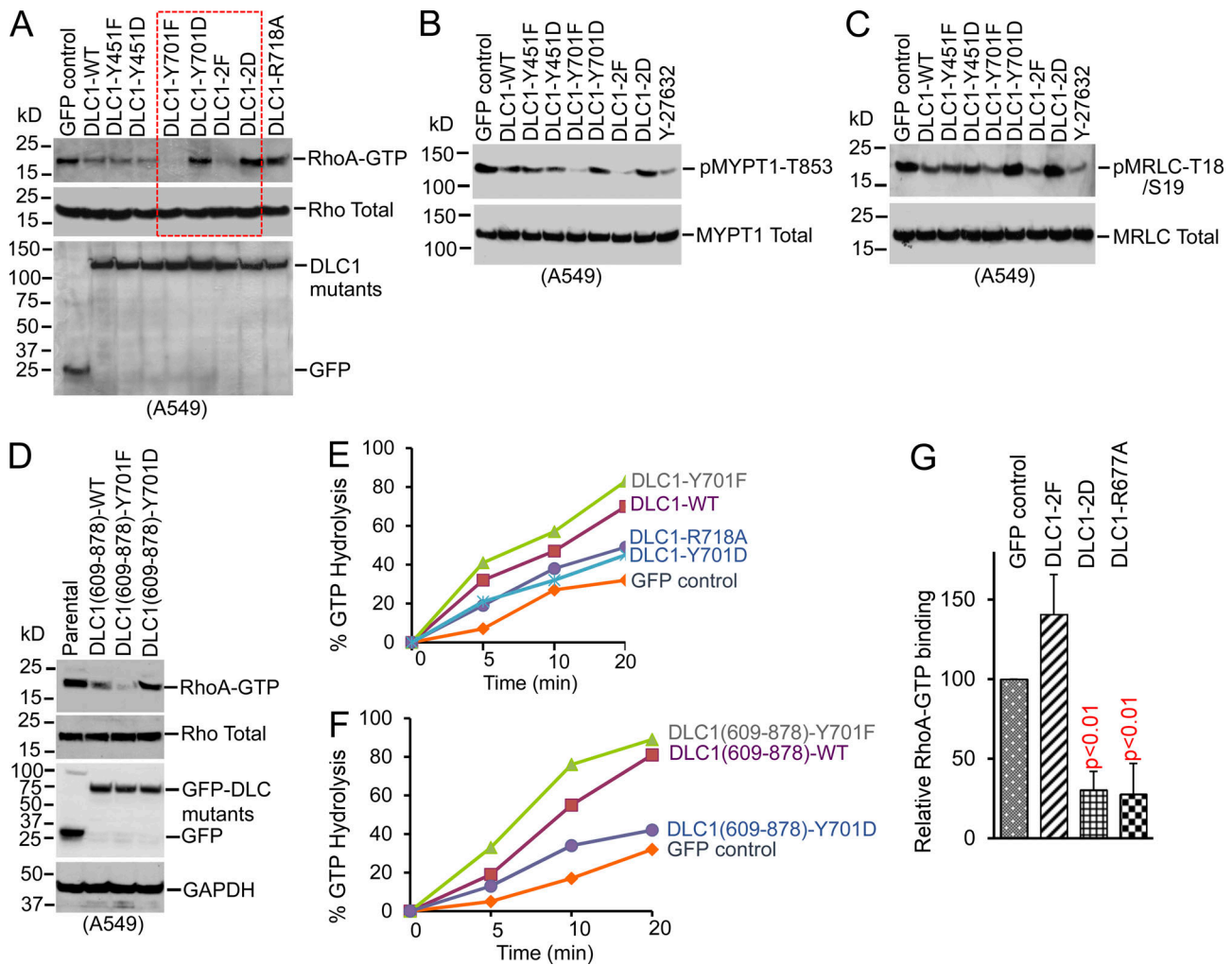
Figure 6.   **SRC phosphorylation of DLC1 attenuates DLC1 Rho-GAP activity. (A)** DLC1 carrying the Y701D mutation has reduced Rho-GAP activity. RhoA-GTP is mainly regulated by DLC1 Y701 phosphorylation (highlighted in red-dotted rectangle). DLC1-Y701D and DLC1-2D mutants are as defective as "GAP-dead" DLC1-R718A mutant for reducing RhoA-GTP, DLC1-2F mutant is more active than DLC1-WT, and DLC1-Y451F and DLC1-Y451D mutants are as active as DLC1-WT. **(B)** pMYPT1-T853 (top), which is a downstream effector for active Rho, and total MYPT1 (bottom) in individual or combined mutants of DLC1. Y27632, a ROCK inhibitor, was used as a positive control. **(C)** pMRLC-T18/S19 (top), which is a downstream marker for active Rho, and total MRLC (bottom) in individual or combined mutants of DLC1. The data in B and C correlate with the RhoA-GTP data shown in A. **(D)** In the isolated Rho-GAP domain (DLC1[609–878]), DLC1 Y701 mutations confer the same RhoA-GTP phenotype in transfected A549 cells as do these mutations in full-length DLC1. The DLC1(609–878)-Y701F mutant reduces RhoA-GTP more efficiently than the DLC1(609–878)-WT, while the DLC1(609–878)-Y701D mutant is defective for reducing RhoA-GTP. **(E and F)** Relative Rho-GAP activity of DLC1 full-length (E) and isolated Rho-GAP domain mutants (F). In vitro RhoA-GTP hydrolysis by indicated DLC1 mutants. Hydrolysis of RhoA-GTP by DLC1-Y701D and DLC1(609–878)-Y701D was similar to GFP control or GAP-dead DLC1-R718A. Hydrolysis of RhoA-GTP by full-length DLC1-Y701F and DLC1(609–878)-Y701F was greater than full-length DLC1-WT and DLC1(609–878)-WT, respectively. These data correlate with the in vivo RhoA-GTP data shown in A and D. **(G)** DLC1-2D binds RhoA-GTP in vitro less efficiently than DLC1-WT or DLC1-2F mutant. DLC1 proteins were partially purified from transfected HEK 293T cells, and bound in vitro to RhoA-GTPγS, a nonhydrolyzable GTP analogue. GAP-dead DLC1-R677A, which is known to reduce binding in this assay (Jaiswal et al., 2014), was included as a control. Graph shows relative RhoA-GTPγS binding to each DLC1 mutant, from three experiments.

higher antitumor activity in the DLC1-WT tumors is attributable to reactivation of DLC1 by the SRC inhibitor. Biochemical analyses of the tumors directly support this inference, as saracatinib treatment reduced RhoA-GTP only in the DLC1-WT line, although SRC activity was inhibited in all lines (Fig. 8, F and G).

Combined AKT and SRC kinase inhibition cooperate to suppress tumor growth

We recently reported that AKT, by directly phosphorylating three specific serines in DLC1, attenuates its tumor suppressor activity and showed that this attenuation could be reversed by

the AKT inhibitor MK-2206 (Tripathi et al., 2017). As these effects of AKT and its inhibition were qualitatively similar to those of SRC and its inhibition, but were clearly attributable to different phosphorylations on DLC1, we asked whether combined inhibition of AKT and SRC might have cooperative effects on tumor inhibition in a cell line that expressed DLC1. To examine this possibility, we compared the antitumor activity of the H358 cell line expressing DLC1-WT with the isogenic DLC1-negative line. In the DLC1-positive line, 5 d of combined treatment with MK-2206 and saracatinib resulted in an 89% decrease in tumor weight, while single-agent treatment reduced tumor weight by
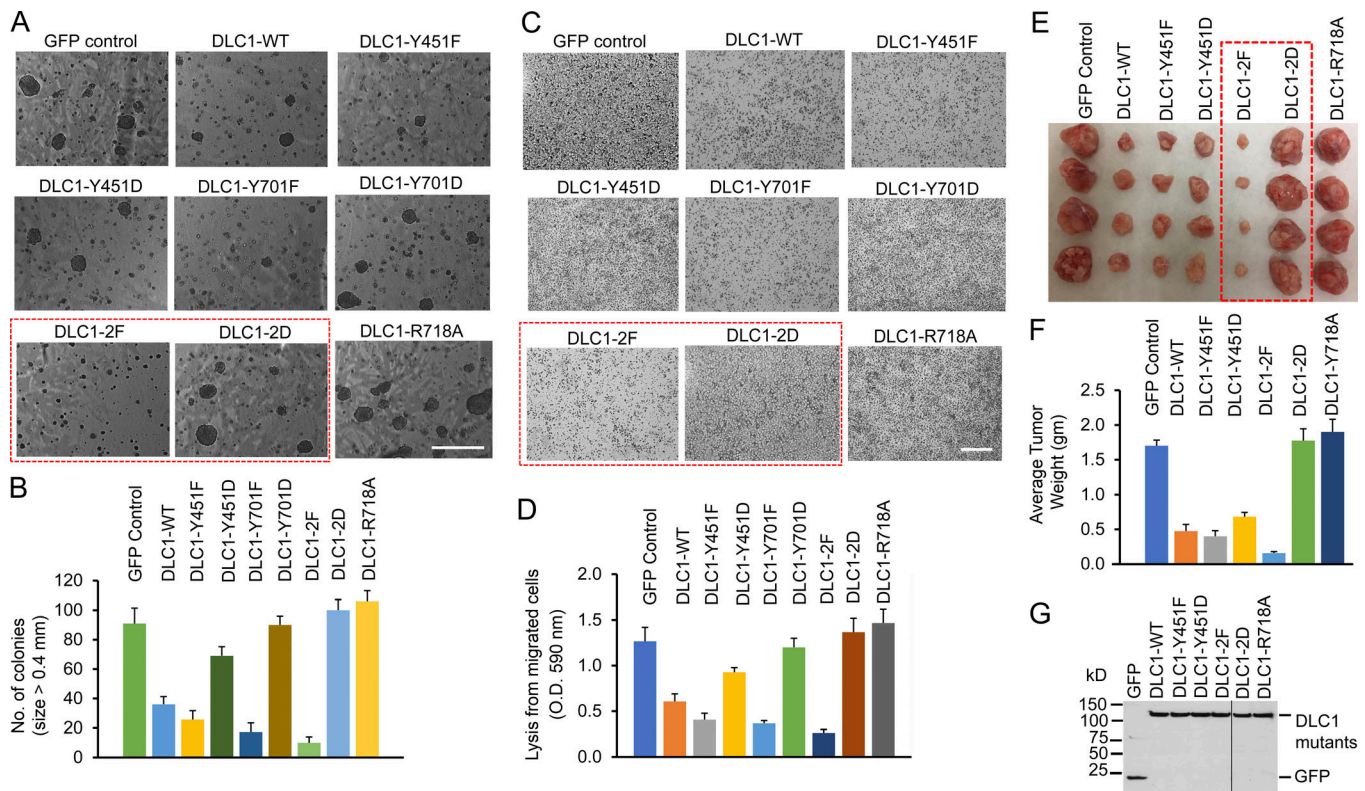
Figure 7. **SRC phosphorylation of DLC1 attenuates its tumor suppressor functions. (A and B)** Anchorage-independent growth: DLC1-2D is as defective as GAP-dead DLC1-R718A; DLC1-2F is even more active than DLC1-WT. **(A)** Photomicrographs of representative agar colonies. Scale bar, 2 mm. **(B)** Quantification of agar colonies (>0.4 mm) from three experiments. **(C and D)** Cell migration: DLC1-2D is as defective as GAP-dead DLC1-R718A; DLC1-2F is more inhibitory than DLC1-WT. **(C)** Photomicrograph of representative migrated cells. Scale bar, 100 mm. **(D)** Graph shows transwell cell migration from three experiments. **(E and F)** Xenograft tumors from mice excised 6 wk after injecting stable transfectants. **(E)** Photographs of excised tumors. **(F)** Graph shows average tumor weight (g) ± SD for each group. DLC1-2D is as defective for tumor suppression as GAP-dead DLC1-R718A. The tumor suppressor activity of DLC1-2F mutant is even greater than DLC1-WT. Red-dotted rectangles in A, C, and E highlight the difference between combined phosphodeficient and combined phosphomimetic mutants. **(G)** Expression of GFP and DLC1 constructs in H358 stable transfectants.

67% for MK-2206 alone and 64% for saracatinib alone (Fig. 9, A and B). These results were correlated with the combination treatment reducing RhoA-GTP to a greater degree than did single-agent treatment (Fig. 9, C and D). In contrast, combined treatment of the DLC1-negative line reduced tumor weight by only 28% and did not result in decreased RhoA-GTP, although inhibition of the AKT and SRC—as determined by pAKT-S473 and pSRC-Y416, respectively—was similar in both lines. The combination treatment induced β-galactosidase and annexin V expression, which are markers of cellular senescence and apoptosis, respectively, to a greater degree than single-agent treatment (Fig. S5, A–D). We also determined that the antitumor activity of two other AKT and tyrosine kinase inhibitors, perifosine and bosutinib, respectively, when used in combination against the two H358 lines, was similar to that found for MK-2206 and saracatinib (Fig. S5, E and F).

Discussion

This study reports several noteworthy observations. We have determined that DLC1 is a major biological and biochemical target of SRC, identified a DLC1-dependent relationship between SRC and RhoA, and demonstrated that enzymatically active SRC

binds and phosphorylates two tyrosines in DLC1. These observations are relevant both to normal physiology and cancer, as they were made in nontransformed lines and in tumor cell lines. In addition, DLC1-S129 lies within amino acids that form both a consensus site for SH3 binding domains and for ERK1/2 phosphorylation; our experimental data confirm that ERK1/2 phosphorylation of DLC1-S129 facilitates the binding of the SRC SH3 domain and full-length SRC to DLC1, which increases the SRC-dependent phosphorylation of DLC1-Y451 and -Y701. Thus, SRC and ERK1/2 signaling converge on DLC1 to cooperatively regulate it, with SRC-dependent phosphorylation of DLC1 attenuating the Rho-GAP– and tensin-binding activities of DLC1 and decreasing its tumor suppressor functions. Although most of our experiments have been focused on SRC, the results are likely to be relevant to other SFKs, as in vitro kinase assays were also positive for FYN and YES. Finally, we began to explore the translational implications of the potential reversibility of the SRC-induced attenuation of DLC1 functions. These experiments show the antitumor activity of a SRC kinase inhibitor is much more potent in DLC1-positive tumors, because the inhibitor reactivates the tumor suppressor activity of DLC1. This observation also underscores the importance of DLC1 as a key biological SRC target in DLC1-positive tumors. Furthermore, we
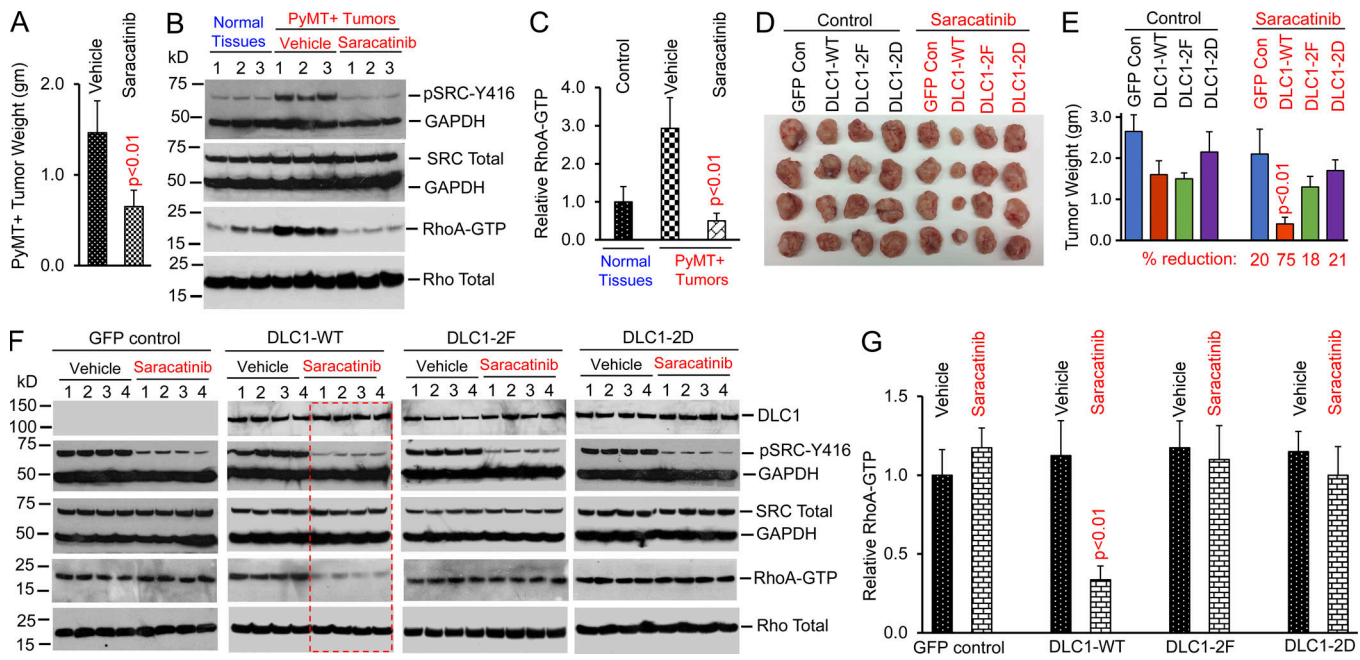
Figure 8.   **SRC inhibitors reactivate DLC1 and have strong antitumor activity in DLC1-positive tumors. (A)** 5 d of saracatinib treatment of MMTV-PyMT mice with breast tumors reduces the weight of breast tumors by >50%. Graph shows average of remaining tumor weight ± SD. **(B)** Compared with breast tissue from pregnant WT mice (normal tissues), MMTV-PyMT tumors treated with the vehicle control have high SRC activity and high RhoA-GTP. 5 d of saracatinib treatment of MMTV-PyMT tumors reduced SRC activity and RhoA-GTP. **(C)** Graph shows relative RhoA-GTP ± SD from each group, as shown in B. **(D and E)** 5 d of saracatinib treatment reduces tumor weight more strongly in DLC1-WT tumors than in isogenic DLC1-negative and DLC1 mutant tumors. Isogenic H358 stable clones expressing GFP control, DLC1-WT, DLC1-2F, or DLC1-2D were injected subcutaneously into NOD-SCID mice. When tumors were ~1.0 cm in diameter, mice were treated with saracatinib for 5 d. **(D)** Tumors from NOD-SCID mice excised after treatment. **(E)** Graph shows the percentage of reduced tumor weight from saracatinib treatment, compared with the vehicle control. Parametric two-tailed t tests were performed for statistical analysis. **(F)** 5 d of saracatinib treatment of tumors shown in C efficiently inhibited SRC activity in all treated tumors, but only reduced RhoA-GTP in DLC1-WT tumors (second panel, highlighted in red-dotted rectangle), and not in DLC1-negative (GFP control, first panel) or DLC1 mutant tumors (third and fourth panels). The apparent similarity in RhoA-GTP for the DLC1-2F and DLC1-2D mutants (third and fourth panels) is caused by the different exposure time. **(G)** Graph shows relative RhoA-GTP ± SD within each group, as shown in F.

demonstrated cooperative antitumor activity from the combined inhibition of SRC and AKT, which phosphorylates and attenuates the tumor suppressor function of DLC1 by a mechanism distinct from that of SRC (Tripathi et al., 2017). A schematic model of the various effects of SRC on DLC1 is shown in Fig. 10.

SRC has been previously reported to regulate RhoA, but its ability to do so has often been attributed to the activation of Rho-specific GEFs or to inactivation of p190–Rho-GAP (Fincham et al., 1999; Huveneers and Danen, 2009; Pullikuth and Catling, 2010). Under both normal steady-state growth conditions and acute integrin activation by fibronectin, the regulation of RhoA-GTP by the SRC kinase was found to be determined primarily by whether or not DLC1 was expressed, rather than by these other regulators, and to depend on DLC1 phosphorylation by SRC. Kinetic analysis of the fibronectin-dependent increase in RhoA-GTP indicated it occurred within minutes of SRC binding and phosphorylating DLC1. Thus, attenuation of DLC1 by its SRC-dependent phosphorylation should be considered when SRC is found to regulate RhoA-GTP. These results complement those we recently reported for AKT, which is downstream of receptor tyrosine kinases, in phosphorylating serines in DLC1 that attenuate its function, including increased RhoA-GTP (Tripathi et al., 2017).

The phylogenetically conserved tyrosines Y451 and Y701 phosphorylated by SRC are strategically located in DLC1 and are conserved in DLC family members DLC2 and DLC3, which we found are also SRC substrates. Y451 lies just downstream from amino acids 440–445, which form part of the docking site for the SH2 domains of tensins and includes Y442, which is required for tensin binding (Liao et al., 2007; Qian et al., 2007). Y451 is also located upstream from the amino acids needed for binding the R8 domain of talin, which have been mapped to DLC1 residues 467–489 (Li et al., 2011; Zacharchenko et al., 2016). Mutating DLC1-Y451 to the phosphomimetic DLC1-D451 led to decreased tensin binding but did not affect talin binding. Y701 lies within the Rho-GAP domain, and the DLC1-Y701D mutant had decreased RhoA-GTP binding and decreased Rho-GAP activity, which strongly implies that these phenotypes are attributable to conformational changes in the Rho-GAP domain induced by Y701 phosphorylation. Consistent with this interpretation, these phenotypes did not require sequences beyond the Rho-GAP domain, as the decreased Rho-GAP activity of Y701D mutant of the isolated Rho-GAP domain (DLC1[609–878]) was similar to that of the same mutant in full-length DLC1. The profound impact of Y701 phosphorylation on Rho-GAP activity contrasts markedly with the phosphorylation by PDK of S807 in the DLC1 Rho-GAP domain, which is reported not to affect Rho-GAP
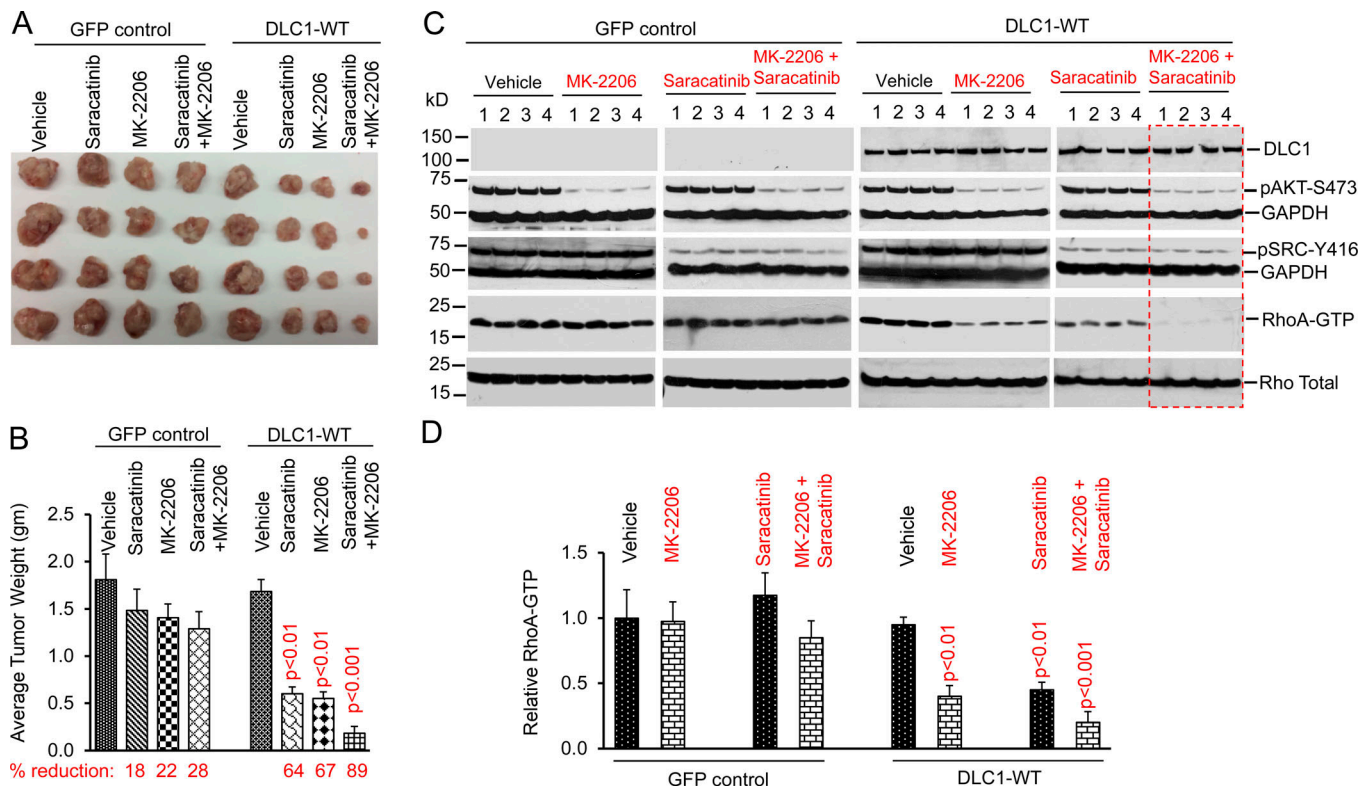
Figure 9. Cooperative antitumor activity from combined treatment with saracatinib and MK-2206 in DLC1-WT tumors. (A and B) H358 xenograft tumors from NOD-SCID mice excised after 5 d of oral treatment with saracatinib alone, MK-2206 alone, or in combination. **(A)** Photographs of excised tumors. **(B)** Graph shows average tumor weight (g) ± SD for each group and the percentage of reduced tumor weight from treatment with saracatinib and/or MK-2206, compared with the vehicle control. **(C)** In the DLC1-WT tumors shown in A, saracatinib alone reduced RhoA-GTP, and MK-2206 alone reduced RhoA-GTP, while combined treatment with saracatinib and MK-2206 reduced RhoA-GTP to an even greater degree than single-agent treatment (fourth panel, highlighted in red-dotted rectangle). These changes in RhoA-GTP were not seen in the GFP control tumors shown in A, although SRC activity (pSRC-Y416) was inhibited similarly in all tumors treated with saracatinib, and AKT activity (pAKT-S473) was inhibited similarly in all tumors treated with MK-2206. **(D)** Graph shows relative RhoA-GTP ± SD from each group, as shown in C.

activity (Scholz et al., 2011). The small degree of residual tyrosine phosphorylation seen in the in vitro SRC kinase assay with the DLC1-2F mutant suggests there might be another tyrosine in DLC1 that is phosphorylated by SRC. However, this putative phosphorylation by SRC would be less efficient than that of Y451 and Y701, and does not by itself appear to alter the Rho-GAP activity of DLC1, as SRC inhibition did not affect this parameter in cells expressing the DLC1-2F and DLC1-2D mutants.

SRC protein in complex with DLC1 is enzymatically active and binds two distinct regions of DLC1, an N-terminal segment of the linker region (amino acids 80–200) and the Rho-GAP domain. The DLC1 N-terminal segment binds the SH3 domain of SRC, which is only available when SRC is active, as this domain forms an intramolecular complex with the SRC kinase domain when SRC is inactive (Espada and Martín-Pérez, 2017). Under our steady-state growth conditions, the colocalization of active SRC with the focal adhesion protein vinculin depended on the presence of DLC1.

The potential reversibility of DLC1 phosphorylation by SRC may have translational implications. SRC kinase inhibitors have been approved by the US Food and Drug Administration for cancer treatment (Roskoski, 2015), but what accounts for the heterogeneity of the clinical responses is frequently

unclear. Our results indicate that SRC kinase inhibition can have strong antitumor activity in two DLC1-positive tumor models with high SRC activity, the MMTV-PyMT breast cancer model and tumor xenografts from a NSCLC line. The responses were associated with decreased tyrosine phosphorylation of DLC1 and decreased RhoA-GTP in tumor extracts. By contrast, if the NSCLC line did not express DLC1, SRC inhibition did not change RhoA-GTP levels and had lower antitumor activity, as was also true of isogenic DLC1 mutants that were not activatable by SRC inhibition because they carried mutations in Y451 and Y701. These results confirm that DLC1 activation in this line is required for the strong antitumor activity of SRC inhibition. Thus, despite there being many SRC substrates, DLC1 can be a sufficiently important one that its reactivation can make a critical contribution to the antitumor activity of SRC inhibitors.

We also demonstrated cooperative antitumor activity from combined treatment of the DLC1-positive NSCLC line with SRC and AKT inhibitors. These results were correlated with the combination inducing lower levels of RhoA-GTP and higher levels of senescence and apoptosis markers than treatment with either inhibitor alone. These observations represent a rigorous proof-of-principle that it might be clinically useful to combine
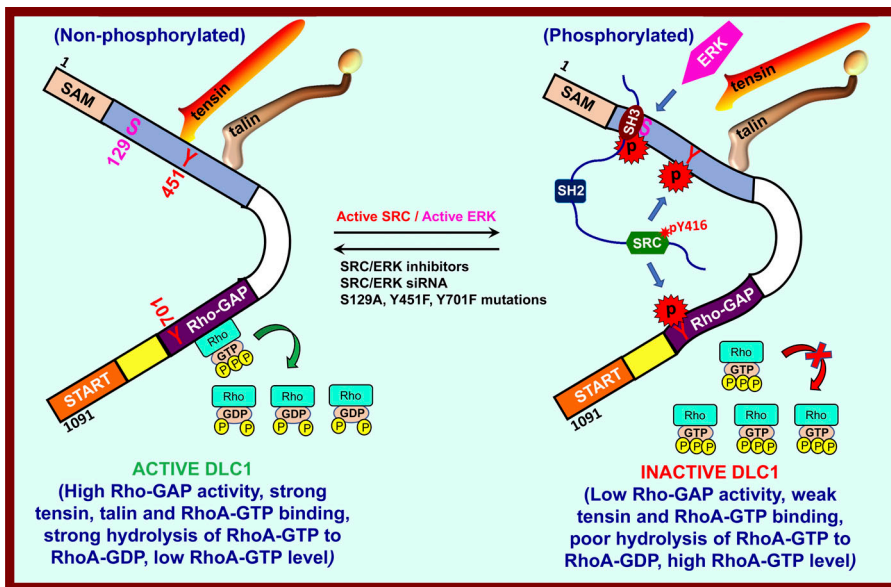
Figure 10. **Model of the regulation of DLC1 by ERK/SRC.** The left side shows that, in the absence of serine (S129) phosphorylation by ERK and tyrosine (Y451 and Y701) phosphorylation by SRC, DLC1 strongly binds tensin protein and RhoA-GTP, and DLC1 has high Rho-GAP activity, which efficiently hydrolyzes the bound RhoA-GTP to RhoA-GDP and resulted in a low RhoA-GTP level in the cell. The right side shows that, in the presence of serine (S129) phosphorylation by ERK, the binding of SRC SH3 to DLC1 is increased, which increases the SRC-dependent phosphorylation of DLC1-Y451 and -Y701. Phosphorylation of DLC-Y451 by SRC inhibits the binding of tensin to DLC1, while phosphorylation of DLC1-Y701 by SRC reduces RhoA-GTP binding to DLC1 and decreases Rho-GAP activity, resulting in poor hydrolysis of RhoA-GTP to RhoA-GDP, which resulted in an increased RhoA-GTP level in the cell. The middle part of model indicates that these phosphorylations are reversible and DLC1 can be activated again by SRC inhibitors, SRC siRNA, or mutation of DLC1 at ERK/SRC phosphorylation sites.

drugs that use distinct mechanisms to reactivate the tumor suppressor activity of DLC1.

Although it is of course critical for inhibitors to hit their target, our data highlight that clinical efficacy can also be critically dependent on the downstream targets affected by the inhibition. Using reactivation of DLC1 as a possible biomarker of clinical efficacy incorporates the impact of oncoprotein inhibition on reactivation of a tumor suppressor, rather than focusing the effects exclusively on the inhibition of pro-oncogenic factors. Such considerations have been usefully applied to the development of CDK4/6 inhibitors, thanks to the basic observation that CDK4/6-dependent phosphorylation of pRB can attenuate its tumor suppressor functions (Sherr et al., 2016). pRB can serve as a biomarker whose decreased phosphorylation and concomitant reactivation are associated with an increased likelihood of clinical response to CDK4/6 inhibitors.

For DLC1, a limitation of the specific therapeutic approach described here is that it is likely to benefit only those tumors that express moderate to high levels of DLC1. However, the down-regulation of DLC1 in many tumors appears to be attributable to epigenetic changes that may be reversible, although DLC1 down-regulation in some tumors arises because of *DLC1* mutation or deletion, which is irreversible (Durkin et al., 2007; Lukasik et al., 2011; Barras and Widmann, 2014; Ko and Ping Yam, 2014; Wang et al., 2016). One possible way to increase the proportion of tumors for which the therapeutic targeting of DLC1 could be clinically beneficial might be to use a suitable inhibitor to reverse an epigenetic change that has resulted in reduced or silenced DLC1 expression at the mRNA or protein level, thus increasing the steady-state level of DLC1 protein, and to combine this treatment with inhibition of SRC and/or AKT kinase activities. This approach could be conceptually relevant for targeting other tumor suppressor genes that are inactivated by several epigenetic mechanisms.

Materials and methods

Plasmid constructs

GFP-tagged DLC1 WT (GFP-DLC1-WT), two DLC1 Rho-GAP–dead mutants (GFP-DLC1-R718A and GFP-DLC1-R677A), and GFP-tagged DLC1 fragments encoding DLC1 residues 1–492, 500–1,091, 1–110, 80–200, 80–300, 80–400, 400–500, 500–700, 609–850, 609–878, 623–1,091, 800–900, 850–1,091, 899–996, 996–1,091, and GFP-DLC3 were constructed by PCR and subcloned into a modified pEGFP-C1 vector through Kpn1-NotI sites, as described (Qian et al., 2007). GST-tagged tensin and talin fragments were described previously (Qian et al., 2007; Li et al., 2011). GFP-DLC2 was a gift from M. Mowat (University of Manitoba, Winnipeg, Canada). A series of individual and combined tyrosine-to-phenylalanine (Y-F), tyrosine-to-aspartate (Y-D), serine-to-alanine (S-A), and serine-to-aspartate (S-D) mutations were introduced into full-length DLC1-WT and into DLC1 fragments using a site-directed mutagenesis kit (Agilent Technologies). Full-length DLC1 and DLC1(80–550) linker region fragments with or without Y451F or Y451D mutation were engineered into the PEBG vector by BamHI and NotI, resulting in GST-tagged DLC1 constructs. All PCR regions were confirmed by sequencing. The sequence for each primer was as follows: DLC1S129A, forward 5′-GACCTG GTCCCTGGGGCCCCAGACGACTCC-3′; DLC1S129A, reverse 5′-GGAGTCGTCTGGGGCCCCAGGGACCAGGTC-3′; DLC1S129D, forward 5′-GACCTGGTCCCTGGGGACCCAGACGACTCC-3′; DLC1S129D, reverse 5′-GGAGTCGTCTGGGTCCCCAGGGACCAGGTC-3′; DLC1Y 451F, forward 5′-GGCTCCATCCTCTTCTCCAGTTCAGGG-3′; DLC1Y451F, reverse 5′-CCCTGAACTGGAGAAGAGGATGGAGCC-3′; DLC1Y451D, forward 5′-GGCTCCATCCTCGACTCCAGTTCAGGG-3′; DLC1Y451D, reverse 5′-CCCTGAACTGGAGTCGAGGATGGAGCC-3′; DLC1Y701F, forward 5′-GACTGTGTCAACTTCGAAGGACAG-3′; DLC1Y701F, reverse 5′-AGACTG TCCTTCGAAGTTGACACAGTC-3′; DLC1Y701D, forward 5′-GACTGTGTC AACGACGAAGGACAGTCT-3′; and DLC1Y701D, reverse 5′-AGACTGTCC TTCGTCGTTGACACAGTC-3′.

Antibodies and fluorescent probes

The following antibodies were obtained from Cell Signaling Technology: SRC rabbit (2108), SRC mouse (2110), phospho-SRC-pY416 (2101), phospho-SRC-pY527 (2105), AKT mouse (2920), AKT rabbit (4691), phospho-AKT-pS473 rabbit (4060), phospho-AKT-pT308 rabbit (13038), phospho-MRLC-Thr18/Ser19 rabbit (3674), MYPT1 (2634), pMYPT1-T853 (4563), FAK rabbit (3285), and GAPDH rabbit (2118). Two DLC1 antibodies, which gave similar results, were used: one generated in our laboratory (DLC1 antibody; clone 428; 24) and the other, DLC1 mouse (612021) antibody, from BD Biosciences. FAK mouse (610088), phospho-FAK-Y397 (611723), and phospho-serine mouse (612547) were purchased from BD Biosciences. EGFR rabbit (ab2430), phospho-EGFR-Y845 rabbit (ab5636), MRLC mouse (ab11082), GFP mouse (ab1218), GFP rabbit (ab290), ERK1 (ab137766), phospho-ERK (ab24157), annexin V (ab14196), and β-galactosidase (ab1047) antibodies were purchased from Abcam. RhoA mouse (ARH04) and phospho-MRLC goat (sc-12896) antibodies were obtained from Cytoskeleton and Santa Cruz Biotechnology, respectively. The phospho-tyrosine mouse (4G10) antibody was obtained from Millipore. The p190–Rho-GAP mouse (R3150) and vinculin (V9131) antibodies were obtained from Sigma-Aldrich. Anti-rabbit (NA934V) and anti-mouse (NXA931V) IgG horseradish peroxidase–linked secondary antibodies were purchased from GE Healthcare. Alexa Fluor 568 anti-rabbit IgG, Alexa Fluor 488 anti-mouse IgG, Alexa Fluor 488 phalloidin, and DAPI were purchased from Invitrogen.

Cell lines, culture conditions, DNA, and siRNAs transfection

HEK 293T, human skin epithelial H2071, human fibroblastic H1634, and HBECs were cultured in DMEM supplemented with 10% FBS. Human NSCLC lines (H1703, H157, A549, and H358) were cultured in RPMI-1640 supplemented with 10% FBS. Transient transfections were performed with Lipofectamine 3000 (Invitrogen) and cultured for 48 h. Stable clones expressing GFP or DLC1 mutants were made by transfecting H1703 or H358 cells with Lipofectamine 3000 followed by G418 selection (0.9 µg/ml). Knockdown of protein expression, with two different siRNAs, was confirmed by IB. Validated siRNAs for human DLC1 (Hs_DLC1 siRNA_5, SI03219909; and Hs_DLC1 siRNA_11, SI04952213), p190–Rho-GAP (Hs_GRLF1 siRNA_7, SI02664025; and Hs_GRLF1 siRNA_8, SI02664032), and SRC (Hs_SRC siRNA_7, SI02223928; and Hs_SRC siRNA_10, SI02664151) were from obtained from QIAGEN, as were negative control siRNAs (control siRNA 1, 1027280; and control siRNA 2, 1027310).

The sequence for each DLC1 siRNA was as follows: Hs_DLC1_5 sense sequence: 5′-CGAUGUCGUAAUUCCUAUATT-3′; Hs_DLC1_5 antisense sequence: 3′-CGGCUACAGCAUUAA GGAUAU-5′; Hs_DLC1_11 sense sequence: 5′-GGAGUGUAGGAA UUGACUATT-3′; and Hs_DLC1_11 antisense sequence: 3′-GAC CUCACAUCCUUAACUGAU-5′.

The sequence for each GRLF1 (p190 Rho-GAP) siRNA was as follows: Hs_GRLF1_7 sense sequence: 5′-GGAUGUUCUGGGAGA GGAATT-3′; Hs_ GRLF1_7 antisense sequence: 3′-GTCCUACAA GACCCUCUCCUU-5′; Hs_ GRLF1_8 sense sequence: 5′-GCCUAA

GGAGGAACACUAATT-3′; and Hs_ GRLF1_8 antisense sequence: 3′-GTCGGAUUCCUCCUUGUGAUU-5′.

The sequence for each SRC siRNA was as follows: Hs_SRC_7 sense sequence: 5′-GCUUGUGGGUGAUGUUUGATT-3′; Hs_ SRC_7 antisense sequence: 3′-GCCGAACACCCACUACAAACU-5′; Hs_ SRC_10 sense sequence: 5′-CCAUGUGCGUCCAUAUUU ATT-3′; and Hs_ SRC_10 antisense sequence: 3′-GAGGUACAC GCAGGUAUAAAU-5′.

siRNA transfection and treatment of cells with fibronectin and inhibitors of SRC and FAK

To reduce the indicated protein expression, cells were transfected with indicated siRNAs (160 nM) or with scrambled control siRNAs and harvested 48 h later. The final concentration of fibronectin (Sigma-Aldrich) was 100 ng/ml. SRC inhibitors saracatinib, bosutinib, PP1, and FAK inhibitor FAK-14 (used at 10 µM each) were purchased from Selleckchem. After overnight incubation in serum-free media, cells were treated with indicated ligand or inhibitors for 15–120 min.

In vitro SRC and ERK kinase assays

Lysates from transfected cells were IP with GFP antibody, and immunopellets were sequentially washed once with high-salt HNTG buffer (20 mM Hepes, 500 mM NaCl, 0.1% Triton X-100, and 10% glycerol), twice with low-salt HNTG buffer (20 mM Hepes, 150 mM NaCl, 0.1% Triton X-100, and 10% glycerol), and once with kinase reaction buffer (35 mM Hepes, pH 7.4, 10 mM $MgCl_2$, 1 mM EGTA, 1% Tween 20, 0.1 mM sodium vanadate, and 1 mM DTT). The kinase reaction was performed in 30 µl of reaction buffer containing 15 µM cold ATP, 2.5 µCi [^{32}P]γ-ATP, and 100 ng of recombinant active SRC, YES, FYN, or ERK1/2 (EMD Millipore) at 30°C for 45 min. The reaction was stopped by adding 10 µl of 4× Laemmli sample buffer and heating at 95°C for 5 min. Proteins were separated by gel electrophoresis and autoradiographed to detect ^{32}P incorporation.

In vivo pull-down assay, coIP, and IB

Cells were transiently cotransfected with plasmids expressing GST or the indicated GST fusion constructs together with GFP or the indicated GFP-DLC1 constructs. 48 h after transfection, cells were lysed with golden lysis buffer (20 mM Tris, pH 7.9, 137 mM NaCl, 10% glycerol, 1% Triton X-100, 5 mM EDTA, 1 mM EGTA, 1 mM Na_3VO_4, 10 mM NaF, 1 mM sodium pyrophosphate, 0.5 mM β-glycerophosphate, protease inhibitor mixture tablet, and phosphatase inhibitor). The cleared supernatants were collected, and a small portion of supernatants was taken to determine the protein concentration using the DC protein assay (Bio-Rad). For the pull-down assay, 1.0 mg of total protein from each cell extracts were used, to which 30 µl of glutathione Sepharose-4B slurry (GE Healthcare) was added, with continuous rotation for 3 h at 4°C. The pellets were sequentially washed once with golden lysis buffer, once with high-salt HNTG buffer, and twice with low-salt HNTG buffer. The beads were incubated with 30 µl Laemmli sample buffer, subjected to 10% SDS-PAGE, transferred onto nitrocellulose membranes (Invitrogen), and detected by IB using specific antibodies. A portion of the cell extracts was used as a loading control to verify expression of the

Tripathi et al.
SRC inhibitors reactivate the tumor suppressor DLC1

Journal of Cell Biology 3072
https://doi.org/10.1083/jcb.201810098

GFP fusion proteins and the GPF control. For coIP experiments, equal amounts of protein from each cell lysates were precleared with protein G slurry (Thermo Fisher Scientific) and then incubated with the indicated antibodies or control IgG for 1 h at RT. After incubation, 30 µl of protein G slurry was added to each immune reaction and rotated at 4°C overnight. The immunopellets were washed three times as above. coIP proteins were eluted by boiling for 5 min in 30 µl Laemmli sample buffer containing 5% (vol/vol) 2-mercaptoethanol. Eluted proteins were resolved on a NuPage 4–12% BisTris gel and detected by IB using specific antibodies. Immunoreactive bands were detected by enhanced chemiluminescence (ECL-Plus; GE Healthcare) using horseradish peroxidase–linked anti-rabbit or anti-mouse secondary antibodies (1:5,000 dilutions).

Immunofluorescent staining
Transiently or stably transfected cells were seeded onto glass chambers, incubated for 24 h, and fixed with 4% paraformaldehyde for 20 min. Fixed cells were permeabilized with 0.25% Triton X-100 in PBS and then blocked with 3% BSA in PBS for 2 h. The cells were incubated with a 1:200 dilution of the indicated primary antibodies at 4°C overnight. After being thoroughly washed in PBS, the cells were incubated with the appropriate 1:250 Alexa Fluor–conjugated secondary antibodies for 1 h. To visualize actin or nuclei, cells were incubated with phalloidin (1:50) or DAPI (1:2,500) for 1 h. After staining, the cells were thoroughly washed with PBS and mounted with gel mounting solution (Biomeda).

Fluorescent confocal microscopy
Confocal microscopy of fluorescent-labeled cells was performed using a microscope (LSM 780; Carl Zeiss) with an excitation wavelength of 488 nm to detect transfected GFP fusion proteins. Alexa Fluor probes were viewed with excitation wavelengths of 488 nm (Alexa Fluor 488) and 568 nm (Alexa Fluor 568). Images were made at RT using photomultiplier tubes with a Plan-Apochromat 63×/1.4 NA oil differential interference contrast objective lens with a 2× magnifier to produce a 125× magnification. The colocalization of two proteins was analyzed by confocal software (ZEN 2012; Carl Zeiss). For quantification of representative morphology in each group, ~15 cells per condition randomly selected from several fields were analyzed. The average Mander's overlapping colocalization coefficient ± SD was calculated and is shown in each panel. The overlapping colocalization coefficients can range from 0 to 1, where 0 means no colocalization and 1 means full colocalization of the two proteins. The images were minimally processed for levels/contrast adjustment in DAPI panels, and the adjustment was done for all images using Adobe Photoshop CC software. The adjustments do not enhance, erase, or misrepresent any information present in the original images.

RhoA-GTP (Rhotekin-RBD pull-down) assay
A Rho activation assay kit (EMD Millipore) was used to measure GTP-bound RhoA, as described (Tripathi et al., 2014). In brief, equal amounts (1,000 µg) of each cell lysate were incubated with 30 µg GST-Rhotekin Rho-binding domain coupled to glutathione-agarose beads for 45 min. Beads were washed three times with washing buffer. Washed samples were subjected to 4–12% SDS-PAGE, transferred onto nitrocellulose membranes, and detected by IB, using RhoA antibody (ARH04 from Cytoskeleton; and 05-778, clone 55, from EMD Millipore).

ROCK assay
Cells were fixed and harvested in 10% trichloroacetic acid containing 10 mM DDT. Pellets were dissolved in 10 µl of 1 M Tris base and mixed with 100 µl of extraction buffer (8 M urea, 2% SDS, 5% sucrose, and 5% 2-mercaptoethanol). Equal amounts of protein from each cell extract were subjected to 10% SDS-PAGE, transferred onto nitrocellulose membranes, and incubated with antibody specific for phospho-myosin binding subunit (phospho-MYPT1-Thr853) or myosin binding subunit (MYPT1), and protein bands were visualized by enhanced chemiluminescence. ROCK activity was expressed as the ratio of phospho-MYPT1 to total MYPT1.

Rho-GAP activity assay
GFP-tagged DLC1 constructs were purified by IP using GFP antibody from transfected cells in a high-stringency buffer (20 mM Tris-HCl, pH 8.0, 100 mM NaCl, 5 mM MgCl$_2$, NP-40 [0.5%], 1 mM DTT, and protease and phosphatase inhibitor). Highly purified Rho was bound to γ-labeled [P^{32}]GTP. The GTPase accelerating activity (Rho-GAP activity) of indicated DLC1 mutants was compared by incubating the DLC1 mutants with GTP-bound RhoA at 18°C with shaking while removing samples at the indicated time points. The guanidine nucleotides were separated by chromatography on cellulose filter paper dissolved in buffer. The γ-P^{32} signal was then determined, and the net GTP hydrolysis was calculated.

PLA
PLA was used to visualize proximity colocalization (<40 nm) of DLC1 and SRC, and kinase-active SRC and vinculin, in NSCLC lines using the Duolink Detection kit (Olink Bioscience). The cells were fixed with 4% PFA for 20 min at RT and then incubated with 0.25% Triton X-100 for 5 min. After blocking with 3% BSA, cells were incubated overnight at 4°C with indicated primary antibodies. After washing, cells were incubated with secondary antibodies with PLA probes (MINUS probe-conjugated anti-rabbit IgGplus PLUS probe-conjugated anti-mouse IgG). Circularization and ligation of the oligonucleotides in the probes were followed by an amplification step. A complementary fluorescent-labeled probe was used to detect the product of rolling circle amplification. Slides were mounted with Duolink II Mounting Medium containing DAPI. Images were obtained with an LSM 780. The number of colocalization PLA dots in cells was counted using ImageJ software.

Mass spectrometry analysis
HEK 293T cells were cotransfected GFP-tagged DLC1-WT constructs with Flag tag, constitutive kinase-active SRC, or kinase-dead SRC, or DLC1-WT–transfected cells were either untreated or treated with the SRC inhibitor saracatinib. Lysates from the cotransfected or treated cells were IP with GFP antibody, and the

immunopellets were resolved on a NuPage 4–12% BisTris gel. The Coomassie-stained DLC1 gel band was destained, and proteins were reduced, alkylated, and digested with trypsin or LysC, as described (Shevchenko et al., 2006). Digested peptides were further desalted using C18 Ziptip (EMD Millipore) and analyzed by an EASY-nLC 1000 nanoHPLC with a C18 Nano Trap Column and an C18 Nano analytical column with a stainless-steel emitter on Nanospray Flex Ion Sources, coupled online with a Q-Exactive mass spectrometer (Thermo Fisher Scientific). Liquid chromatography–tandem mass spectrometry data were searched against DLC1 protein sequence and human protein database using Proteome Discoverer 1.4 with variable modifications of carbamidomethylation, oxidation of methionine, and phosphorylation of serine, threonine, and tyrosine residues. For legitimate peptide identifications, we applied protein percolator with 1% false discovery rate cutoff (Elias and Gygi, 2010).

Soft agar and anchorage-independent growth assay

For soft agar assays, a 0.6% agar (BD Biosciences) base in RPMI-1640 medium was placed in 60-mm dishes for 1 h at RT. 10^5 cells were mixed with complete medium containing 0.4% agar and placed over 0.6% basal agar in 60-mm dishes. Cells were grown in 0.9 µg/ml G418 RPMI-1640 medium with 10% FBS for 3 wk, and colonies were fixed, stained, photographed microscopically, and quantified with a colony counter.

Cell migration assay

Cell migration was measured by 6.5-mm-diameter Falcon cell culture inserts (8 µm pore size; BD Biosciences). Transiently transfected cells or stable clones were trypsinized, resuspended in serum-free RPMI-1640 medium, and transferred to the upper chamber (7.5×10^4 cells in 300 µl). 600 µl of 10% FBS in RPMI-1640 was placed in the lower chamber. After an 18-h incubation, the cells remaining on the upper surface of insert were removed three times with a cotton swab moistened in PBS. Migrated cells on the lower surface were fixed in methanol for 20 min at RT followed by staining with 2% crystal violet (Sigma-Aldrich) in methanol for 30 min, distained, examined, and photographed by microscopy. For quantification, migrated cells were solubilized with 1% Triton X-100 and counted in a spectrophotometer at OD 590 nm.

In vivo tumorigenesis and treatment of mice with SRC inhibitor

The mouse studies were approved by the National Cancer Institute Animal Care and Use Committee and conducted in compliance with the approved protocols. For tumor xenograft studies, H358 stable clones expressing GFP, GFP-tagged DLC1-WT, DLC1-Y451F, DLC1-Y451D, DLC1-Y701F, DLC1-Y701D, DLC1-2F, DLC1-2D, and DLC1-R718A were trypsinized, washed with cold PBS, diluted to 10^8 cells/ml with serum-free medium/Matrigel basement membrane matrix (BD Biosciences) at a ratio of 3:1, and injected subcutaneously into NOD-SCID mice (10^7 cells/injection). The animals were monitored for tumor growth, and tumor masses were weighed (in grams) 6 wk after injection.

For the treatment of mice with xenograft tumors, H358 stable clones expressing indicated GFP-tagged DLC1 constructs were trypsinized, washed with cold PBS, diluted to 10^8 cells/ml with serum-free medium/Matrigel basement membrane matrix (BD Biosciences) at a ratio of 3:1, and injected subcutaneously into NOD-SCID mice (10^7 cells/injection for GFP control and DLC1-2D groups; 5.0×10^7 cells/injection for DLC1-WT and DLC1-2F groups). When tumors were 1.0–1.5 cm, mice were treated with SRC inhibitor, AKT inhibitor, and a combination of both drugs orally with 50 mg/kg or vehicle control for 5 d, and the remaining tumor tissues were then excised, weighed, and processed for biochemical assays. For MMTV-PyMT mice, tumors were randomly divided into two groups. Mice were treated orally with 50 mg/kg SRC inhibitor or vehicle control for five consecutive days. The remaining tumor tissues were then excised, weighed, and processed for biochemical assays.

Data analysis

At least two independent experiments were performed for all in vitro experiments. IBs were quantified by densitometric scanning using ImageQuant software. Results are expressed as mean densities ± SD from two or three experiments. All experiments were designed with matched control conditions within each experiment. Data distribution was assumed to be normal, but this was not formally tested. For statistical analysis, parametric two-tailed t tests were performed using Prism software (version 7.0a; GraphPad), and $P < 0.05$ was considered statistically significant.

Online supplemental material

Fig. S1 shows that SRC activity increases RhoA-GTP through DLC1. Fig. S2 shows that SRC colocalizes with DLC1, kinase-active SRC (pSRC-Y416) colocalizes with focal adhesion protein vinculin, and LPA increases RhoA-GTP independently of DLC1. Fig. S3 shows the SRC-dependent phosphorylation of the two tyrosines in DLC1 (Y451 and Y701) by mass spectrometry, and all three members of the DLC gene family, *DLC1*, *DLC2*, and *DLC3*, are SRC substrates. Fig. S4 shows that RhoA-GTP and its downstream effectors are regulated by SRC phosphorylation of DLC1. Fig. S5 shows that saracatinib and MK-2206 treatment induces cellular senescence and apoptosis in DLC1-WT tumors, and combined treatment with bosutinib and perifosine suppressed tumor growth more strongly than the individual inhibitors.

JCB

References

Barras, D., and C. Widmann. 2014. GAP-independent functions of DLC1 in metastasis. *Cancer Metastasis Rev.* 33:87–100. https://doi.org/10.1007/s10555-013-9458-0

Buscà, R., J. Pouysségur, and P. Lenormand. 2016. ERK1 and ERK2 Map Kinases: Specific Roles or Functional Redundancy? *Front. Cell Dev. Biol.* 4:53–75. https://doi.org/10.3389/fcell.2016.00053

Destaing, O., A. Sanjay, C. Itzstein, W.C. Horne, D. Toomre, P. De Camilli, and R. Baron. 2008. The tyrosine kinase activity of c-Src regulates actin dynamics and organization of podosomes in osteoclasts. *Mol. Biol. Cell.* 19:394–404. https://doi.org/10.1091/mbc.e07-03-0227

Durkin, M.E., V. Ullmannova, M. Guan, and N.C. Popescu. 2007. Deleted in liver cancer 3 (DLC-3), a novel Rho GTPase-activating protein, is downregulated in cancer and inhibits tumor cell growth. *Oncogene.* 26:4580–4589. https://doi.org/10.1038/sj.onc.1210244

Elias, J.E., and S.P. Gygi. 2010. Target-decoy search strategy for mass spectrometry-based proteomics. *Methods Mol. Biol.* 604:55–71. https://doi.org/10.1007/978-1-60761-444-9_5

Ellenbroek, S.I., and J.G. Collard. 2007. Rho GTPases: functions and association with cancer. *Clin. Exp. Metastasis.* 24:657–672. https://doi.org/10.1007/s10585-007-9119-1

Espada, J., and J. Martín-Pérez. 2017. An Update on Src Family of Nonreceptor Tyrosine Kinases Biology. *Int. Rev. Cell Mol. Biol.* 331:83–122. https://doi.org/10.1016/bs.ircmb.2016.09.009

Fincham, V.J., A. Chudleigh, and M.C. Frame. 1999. Regulation of p190 RhoGAP by v-Src is linked to cytoskeletal disruption during transformation. *J. Cell Sci.* 112:947–956.

Frame, M.C., V.J. Fincham, N.O. Carragher, and J.A. Wyke. 2002. v-Src's hold over actin and cell adhesions. *Nat. Rev. Mol. Cell Biol.* 3:233–245. https://doi.org/10.1038/nrm779

Guy, C.T., S.K. Muthuswamy, R.D. Cardiff, P. Soriano, and W.J. Muller. 1994. Activation of the c-Src tyrosine kinase is required for the induction of mammary tumors in transgenic mice. *Genes Dev.* 8:23–32. https://doi.org/10.1101/gad.8.1.23

Harburger, D.S., and D.A. Calderwood. 2009. Integrin signalling at a glance. *J. Cell Sci.* 122:159–163. https://doi.org/10.1242/jcs.018093

Huveneers, S., and E.H. Danen. 2009. Adhesion signaling - crosstalk between integrins, Src and Rho. *J. Cell Sci.* 122:1059–1069. https://doi.org/10.1242/jcs.039446

Jaiswal, M., R. Dvorsky, E. Amin, S.L. Risse, E.K. Fansa, S.C. Zhang, M.S. Taha, A.R. Gauhar, S. Nakhaei-Rad, K. Kordes, et al. 2014. Functional crosstalk between ras and rho pathways: a Ras-specific GTPase-activating protein (p120RasGAP) competitively inhibits the RhoGAP activity of deleted in liver cancer (DLC) tumor suppressor by masking the catalytic arginine finger. *J. Biol. Chem.* 289:6839–6849. https://doi.org/10.1074/jbc.M113.527655

Kim, T.Y., K.D. Healy, C.J. Der, N. Sciaky, Y.J. Bang, and R.L. Juliano. 2008. Effects of structure of Rho GTPase-activating protein DLC-1 on cell morphology and migration. *J. Biol. Chem.* 283:32762–32770. https://doi.org/10.1074/jbc.M800617200

Klinghoffer, R.A., C. Sachsenmaier, J.A. Cooper, and P. Soriano. 1999. Src family kinases are required for integrin but not PDGFR signal transduction. *EMBO J.* 18:2459–2471. https://doi.org/10.1093/emboj/18.9.2459

Ko, F.C., and J.W. Ping Yam. 2014. Regulation of deleted in liver cancer 1 tumor suppressor by protein-protein interactions and phosphorylation. *Int. J. Cancer.* 135:264–269. https://doi.org/10.1002/ijc.28505

Li, G., X. Du, W.C. Vass, A.G. Papageorge, D.R. Lowy, and X. Qian. 2011. Full activity of the deleted in liver cancer 1 (DLC1) tumor suppressor depends on an LD-like motif that binds talin and focal adhesion kinase (FAK). *Proc. Natl. Acad. Sci. USA.* 108:17129–17134. https://doi.org/10.1073/pnas.1112122108

Liao, Y.C., L. Si, R.W. deVere White, and S.H. Lo. 2007. The phosphotyrosine-independent interaction of DLC-1 and the SH2 domain of cten regulates focal adhesion localization and growth suppression activity of DLC-1. *J. Cell Biol.* 176:43–49. https://doi.org/10.1083/jcb.200608015

Lowell, C.A., and P. Soriano. 1996. Knockouts of Src-family kinases: stiff bones, wimpy T cells, and bad memories. *Genes Dev.* 10:1845–1857. https://doi.org/10.1101/gad.10.15.1845

Lukasik, D., E. Wilczek, A. Wasiutynski, and B. Gornicka. 2011. Deleted in liver cancer protein family in human malignancies (Review). *Oncol. Lett.* 2:763–768.

Meng, X.N., Y. Jin, Y. Yu, J. Bai, G.Y. Liu, J. Zhu, Y.Z. Zhao, Z. Wang, F. Chen, K.Y. Lee, and S.B. Fu. 2009. Characterisation of fibronectin-mediated FAK signalling pathways in lung cancer cell migration and invasion. *Br. J. Cancer.* 101:327–334. https://doi.org/10.1038/sj.bjc.6605154

Moran, M.F., P. Polakis, F. McCormick, T. Pawson, and C. Ellis. 1991. Protein-tyrosine kinases regulate the phosphorylation, protein interactions, subcellular distribution, and activity of p21ras GTPase-activating protein. *Mol. Cell. Biol.* 11:1804–1812. https://doi.org/10.1128/MCB.11.4.1804

Pullikuth, A.K., and A.D. Catling. 2010. Extracellular signal-regulated kinase promotes Rho-dependent focal adhesion formation by suppressing p190A RhoGAP. *Mol. Cell. Biol.* 30:3233–3248. https://doi.org/10.1128/MCB.01178-09

Qian, X., G. Li, H.K. Asmussen, L. Asnaghi, W.C. Vass, R. Braverman, K.M. Yamada, N.C. Popescu, A.G. Papageorge, and D.R. Lowy. 2007. Oncogenic inhibition by a deleted in liver cancer gene requires cooperation between tensin binding and Rho-specific GTPase-activating protein activities. *Proc. Natl. Acad. Sci. USA.* 104:9012–9017. https://doi.org/10.1073/pnas.0703033104

Ren, X.D., W.B. Kiosses, and M.A. Schwartz. 1999. Regulation of the small GTP-binding protein Rho by cell adhesion and the cytoskeleton. *EMBO J.* 18:578–585. https://doi.org/10.1093/emboj/18.3.578

Reynolds, A.B., S.B. Kanner, A.H. Bouton, M.D. Schaller, S.A. Weed, D.C. Flynn, and J.T. Parsons. 2014. SRChing for the substrates of Src. *Oncogene.* 33:4537–4547. https://doi.org/10.1038/onc.2013.416

Roskoski, R. Jr. 2015. Src protein-tyrosine kinase structure, mechanism, and small molecule inhibitors. *Pharmacol. Res.* 94:9–25. https://doi.org/10.1016/j.phrs.2015.01.003

Scholz, R.P., J.O. Gustafsson, P. Hoffmann, M. Jaiswal, M.R. Ahmadian, S.A. Eisler, P. Erlmann, S. Schmid, A. Hausser, and M.A. Olayioye. 2011. The tumor suppressor protein DLC1 is regulated by PKD-mediated GAP domain phosphorylation. *Exp. Cell Res.* 317:496–503. https://doi.org/10.1016/j.yexcr.2010.11.003

Sen, B., and F.M. Johnson. 2011. Regulation of SRC family kinases in human cancers. *J. Signal Transduct.* 2011:865819. https://doi.org/10.1155/2011/865819

Sherr, C.J., D. Beach, and G.I. Shapiro. 2016. Targeting CDK4 and CDK6: From Discovery to Therapy. *Cancer Discov.* 6:353–367. https://doi.org/10.1158/2159-8290.CD-15-0894

Shevchenko, A., H. Tomas, J. Havlis, J.V. Olsen, and M. Mann. 2006. In-gel digestion for mass spectrometric characterization of proteins and proteomes. *Nat. Protoc.* 1:2856–2860. https://doi.org/10.1038/nprot.2006.468

Sulzmaier, F.J., C. Jean, and D.D. Schlaepfer. 2014. FAK in cancer: mechanistic findings and clinical applications. *Nat. Rev. Cancer.* 14:598–610. https://doi.org/10.1038/nrc3792

Takahashi, M., Y. Li, T.J. Dillon, Y. Kariya, and P.J.S. Stork. 2017. Phosphorylation of the C-Raf N region promotes Raf dimerization. *Mol. Cell. Biol.* 37:e00132-e17. https://doi.org/10.1128/MCB.00132-17

Tripathi, B.K., X. Qian, P. Mertins, D. Wang, A.G. Papageorge, S.A. Carr, and D.R. Lowy. 2014. CDK5 is a major regulator of the DLC1. *J. Cell Biol.* 207:627–642. https://doi.org/10.1083/jcb.201405105

Tripathi, B.K., T. Grant, X. Qian, M. Zhou, P. Mertins, D. Wang, A.G. Papageorge, S.G. Tarasov, K.W. Hunter, S.A. Carr, and D.R. Lowy. 2017. Receptor tyrosine kinase activation of RhoA is mediated by AKT phosphorylation of DLC1. *J. Cell Biol.* 216:4255–4270. https://doi.org/10.1083/jcb.201703105

Wang, D., X. Qian, M. Rajaram, M.E. Durkin, and D.R. Lowy. 2016. DLC1 is the principal biologically-relevant down-regulated DLC family member in several cancers. *Oncotarget.* 7:45144–45157.

Webb, D.J., K. Donais, L.A. Whitmore, S.M. Thomas, C.E. Turner, J.T. Parsons, and A.F. Horwitz. 2004. FAK-Src signalling through paxillin, ERK and

eJCB

MLCK regulates adhesion disassembly. *Nat. Cell Biol.* 6:154–161. https://doi.org/10.1038/ncb1094

Wong, C.M., J.W. Yam, Y.P. Ching, T.O. Yau, T.H. Leung, D.Y. Jin, and I.O. Ng. 2005. Rho GTPase-activating protein deleted in liver cancer suppresses cell proliferation and invasion in hepatocellular carcinoma. *Cancer Res.* 65:8861–8868. https://doi.org/10.1158/0008-5472.CAN-05-1318

Xiang, S.Y., S.S. Dusaban, and J.H. Brown. 2013. Lysophospholipid receptor activation of RhoA and lipid signaling pathways. *Biochim. Biophys. Acta.* 1831:213–222. https://doi.org/10.1016/j.bbalip.2012.09.004

Yoon, S., and R. Seger. 2006. The extracellular signal-regulated kinase: multiple substrates regulate diverse cellular functions. *Growth Factors.* 24:21–44. https://doi.org/10.1080/02699050500284218

Zacharchenko, T., X. Qian, B.T. Goult, D. Jethwa, T.B. Almeida, C. Ballestrem, D.R. Critchley, D.R. Lowy, and I.L. Barsukov. 2016. LD Motif Recognition by Talin: Structure of the Talin-DLC1 Complex. *Structure.* 24:1130–1141. https://doi.org/10.1016/j.str.2016.04.016

Zhou, X., and Y. Zheng. 2013. Cell type-specific signaling function of RhoA GTPase: lessons from mouse gene targeting. *J. Biol. Chem.* 288:36179–36188. https://doi.org/10.1074/jbc.R113.515486